Atmospheric Environment 52 (2012) 29–47

Contents lists available at SciVerse ScienceDirect

Atmospheric Environment

journal homepage: www.elsevier.com/locate/atmosenv

An update on polar aerosol optical properties using POLAR-AOD and other measurements performed during the International Polar Year

Claudio Tomasi [a,*], Angelo Lupi [a], Mauro Mazzola [a], Robert S. Stone [b,c], Ellsworth G. Dutton [b], Andreas Herber [d], Vladimir F. Radionov [e], Brent N. Holben [f], Mikhail G. Sorokin [g], Sergey M. Sakerin [h], Svetlana A. Terpugova [h], Piotr S. Sobolewski [i], Christian Lanconelli [a], Boyan H. Petkov [a], Maurizio Busetto [a], Vito Vitale [a]

[a] Institute of Atmospheric Sciences and Climate, Consiglio Nazionale delle Ricerche, Bologna 40129, Italy
[b] Global Monitoring Division (GMD), Earth System Research Laboratory (ESRL), National Oceanic and Atmospheric Administration (NOAA), Boulder, CO, USA
[c] Cooperative Institute for Research in Environmental Sciences, University of Colorado, Boulder, CO, USA
[d] Climate System Division, Alfred Wegener Institute for Polar and Marine Research, Bremerhaven, Germany
[e] Arctic and Antarctic Research Institute (AARI), St. Petersburg, Russia
[f] Biospheric Sciences Branch, NASA Goddard Space Flight Center, Greenbelt, MD, USA
[g] Sigma Space Corp., Biospheric Sciences Branch, NASA's Goddard Space Flight Center, Greenbelt, MD, USA
[h] V.E. Zuev Institute of Atmospheric Optics, Siberian Branch (IAO-SB), Russian Academy of Sciences (RAS), Tomsk, Russia
[i] Institute of Geophysics, Polish Academy of Sciences (PAS), Warsaw, Poland

ARTICLE INFO

Article history:
Received 31 March 2011
Received in revised form
13 February 2012
Accepted 14 February 2012

Keywords:
Polar aerosol optical depth
Long-term AOD variations
Ångström exponent variations
Polar aerosol chemical composition
Polar aerosol radiative parameters
Arctic haze
Volcanic aerosol effects

ABSTRACT

An updated set of time series of derived aerosol optical depth (AOD) and Ångström's exponent α from a number of Arctic and Antarctic stations was analyzed to determine the long-term variations of these two parameters. The Arctic measurements were performed at Ny-Ålesund (1991–2010), Barrow (1977–2010) and some Siberian sites (1981–1991). The data were integrated with Level 2.0 AERONET sun-photometer measurements recorded at Hornsund, Svalbard, and Barrow for recent years, and at Tiksi for the summer 2010. The Antarctic data-set comprises sun-photometer measurements performed at Mirny (1982–2009), Neumayer (1991–2004), and Terra Nova Bay (1987–2005), and at South Pole (1977–2010). Analyses of daily mean AOD were made in the Arctic by (i) adjusting values to eliminate volcanic effects due to the El Chichón, Pinatubo, Kasatochi and Sarychev eruptions, and (ii) selecting the summer background aerosol data from those affected by forest fire smoke. Nearly null values of the long-term variation of summer background AOD were obtained at Ny-Ålesund (1991–2010) and at Barrow (1977–2010). No evidence of important variations in AOD was found when comparing the monthly mean values of AOD measured at Tiksi in summer 2010 with those derived from multi-filter actinometer measurements performed in the late 1980s at some Siberian sites. The long-term variations of seasonal mean AOD for Arctic Haze (AH) conditions and AH episode seasonal frequency were also evaluated, finding that these parameters underwent large fluctuations over the 35-year period at Ny-Ålesund and Barrow, without presenting well-defined long-term variations. A characterization of chemical composition, complex refractive index and single scattering albedo of ground-level aerosol polydispersions in summer and winter–spring is also presented, based on results mainly found in the literature.

The long-term variation in Antarctic AOD was estimated to be stable, within ±0.10% per year, at the three coastal sites, and nearly null at South Pole, where a weak increase was only recently observed, associated with an appreciable decrease in α, plausibly due to the formation of thin stratospheric layers of ageing volcanic particles. The main characteristics of chemical composition, complex refractive index and single scattering albedo of Antarctic aerosols are also presented for coastal particles sampled at Neumayer and Terra Nova Bay, and continental particles at South Pole.

* Corresponding author. Tel.: +39 051 639 9594; fax: +39 051 639 9652.
E-mail address: c.tomasi@isac.cnr.it (C. Tomasi).

1352-2310/$ – see front matter © 2012 Elsevier Ltd. All rights reserved.
doi:10.1016/j.atmosenv.2012.02.055

1. Introduction

Atmospheric aerosols are known to play an important role in changing the radiation budget of the surface-atmosphere system, inducing both direct and indirect radiative effects (Charlson et al., 1992). Direct effects are mainly caused by aerosols through the scattering and absorption of incoming solar radiation, and therefore depend not only on the aerosol burden and radiative properties but also on the surface reflectance characteristics (Chylek and Coakley, 1974). Various indirect effects are caused by aerosols, which act as condensation nuclei that favour the formation of smaller cloud droplets, thus enhancing cloud brightness and modifying the atmospheric life-time of clouds (Schwartz et al., 1995). Surface albedo generally exhibits rather high values in Polar regions covered by snow and ice. Optically dense layers of aerosols and haze particles may therefore induce important changes in the radiation budget of the atmosphere (Randles et al., 2004), and in the overall albedo of the surface-atmosphere system. This quantity varies significantly as a function of solar zenith angle, surface reflectance, and radiative, chemical composition and morphological characteristics of the columnar aerosol particle polydispersions (Shaw et al., 1993; Blanchet, 1995). Empirical analyses, however, show that Arctic aerosols radiatively cool the surface, even when snow covered (e.g., Stone et al., 2007, 2008). Realistic simulations of aerosol radiative forcing at the top of the atmosphere (TOA) and at the surface can only be obtained knowing the aerosol optical depth (AOD), radiative properties of aerosols (such as the complex refractive index and single scattering albedo) and spectral and angular dependence features of the non-lambertian surface reflectance (Ricchiazzi et al., 2005). An improved knowledge of the optical and chemical parameters of polar aerosols is therefore a fundamental pre-requisite for characterizing particle polydispersions of different origin and obtaining realistic estimates of the aerosol radiative impact on climate in the Polar regions. This objective has gained in importance over the past decades, because a marked decrease in the annual average albedo has been observed mainly in the Arctic region since the '80s, due to the gradually increasing sea ice melting in summer and a marked reduction in the snow cover (Stone et al., 2002; Serreze et al., 2003; Holland et al., 2006).

To better define the radiative properties of polar aerosols, Tomasi et al. (2007) analyzed a large set of AOD measurements performed over the last 30 years at numerous Arctic and Antarctic sites using filtered actinometers, multi-filter pyrheliometers and multispectral sun-photometers. Three time series of summer AOD measurements obtained for clean-air conditions at Barrow (from 1977 to 2002), Ny-Ålesund (from 1991 to 2006), and five Siberian Arctic sites (from 1981 to 1991) were analyzed to determine the long-term average variations in AOD and Ångström's atmospheric turbidity parameters over the last three decades, finding negative values of the yearly long-term average trend of summer-time AOD, equal to −1.6% at Barrow, −2.2% at Ny-Ålesund, and −7.6% at the Siberian sites. The decreases were attributed mainly to the diminishing anthropogenic emissions of SO_2, observed especially since 1985 in Europe and Russia, and to the large year-to-year changes in atmospheric transport of anthropogenic aerosols from Europe and Asia (Jaffe et al., 1995), possibly associated with variations in atmospheric circulation patterns that affect cloudiness, temperature and snowfall (Stone, 1997; Stone et al., 2002). The time series of the daily mean values of AOD measured at seven Arctic stations from 1991 to 2006 were analyzed by Tomasi et al. (2007) for the purpose of providing an overall evaluation of the variability of Arctic Haze (hereinafter referred to as AH) formation processes during the winter–spring period at the various sites. Conversely, no evidence was found of significant AOD variations at Antarctic sites.

The long-term variations of Arctic AOD and other sets of satellite-derived and surface-based measurements of AOD on the global scale were analyzed by Chylek et al. (2007), who found an average annual decrease in planetary AOD of about 0.14% per year (y^{-1}), illustrating the great value in long-term monitoring of AOD and aerosol radiative parameters at representative remote sites, and the need to update time series analyses on a regular basis. The present study analyzes the updated time series of AOD and Ångström's exponent α measured over the past 35 years at a number of strategic Arctic and Antarctic sites, including those measurements made during International Polar Year 2007–2009 as part of the POLAR-AOD activity aimed at "characterizing the means, variability and trends of the climate-forcing properties of aerosols in Polar regions" (see http://classic.ipy.org/development/eoi/details.php?id=299). Therefore, field data and measurements taken from the relevant literature are incorporated, to describe the radiative properties of aerosol particles in the Arctic and Antarctic regions.

2. Long-term variations in aerosol optical depth at Arctic sites

Before examining the time series of AOD recorded at the Arctic and Antarctic sites and illustrating the novelty of their analysis, it is useful to describe the procedure adopted by Tomasi et al. (2007) to analyze the long-term variations of AOD in the Arctic. The AOD measurements were performed at:

(i) Ny-Ålesund, in the northern part of Spitsbergen (Svalbard, Norway), where regular multispectral measurements were performed by the AWI (Alfred Wegener Institute, Bremerhaven, Germany) group, using the two sun-photometers and the star-photometer described in Table 1 over the 16-year period from 1991 to 2006 (Herber et al., 1993, 2002);
(ii) Barrow, Alaska, on the coast of the Arctic Ocean, where the NOAA/GMD (National Oceanic and Atmospheric Administration, Global Monitoring Division, Earth System Research Laboratory, Boulder, Colorado) group carried out routine measurements of aerosol optical depth at a mean visible wavelength (AOD_{FWNIP}), performed using Filter Wheel Normal Incidence Pyrheliometer (FWNIP) models over the 25-year period from April 1977 to March 2001 (Dutton and Christy, 1992; Dutton et al., 2004) and spectral observations beginning in 2000 (Stone, 2002) ; and
(iii) Dikson Island, Severnaya Zemlya, Kotel'ny Island, and Wrangel Island, all situated along the Siberian coast of the Arctic Ocean, where the AARI group (Arctic and Antarctic Research Institute, St. Petersburg, Russia) recorded time series of monthly mean values of AOD_{act} in the visible, using thermoelectric narrow-band filtered actinometers over the 11-year period from March 1981 to June 1991 (Radionov and Marshunova, 1992; Radionov, 2005).

Examining the above sets of daily AOD measurements, Tomasi et al. (2007) determined three series of monthly mean values of AOD by first discarding the AOD data recorded during the 1982–1984 and 1992–1994 periods, because they were strongly affected by stratospheric particle extinction effects due to the El Chichón and Pinatubo eruptions, respectively. Subsequently, only the data relative to the four summer months from June to September were considered when calculating the long-term variations of AOD, with the background contribution hereafter referred to as BG, and enhancements attributed to extinction mainly by smoke particles from boreal forest fires (hereafter referred to as FFS) in North America and Siberia (Forster et al., 2001; Damoah et al., 2004; Stohl et al., 2006; Tunved et al., 2006). Following the

Table 1
Main instrumental characteristics of the sun-photometers and star-photometer employed by the AWI group at Ny-Ålesund (Svalbard, Norway), and of the two sun-photometers used by the NOAA/GMD group, of which the SP02 model was employed at Barrow and South Pole from 2001 to 2010, and the SP022 model at Barrow since 2007. The peak wavelengths in bold characters refer to the narrow-band interference filters of the AWI sun-photometers used to determine the spectral values of AOD, while the peak wavelengths in brackets are those used to measure precipitable water.

Instrumental characteristics	Instruments				
	SP-AWI sun-photometers and star-photometer (Herber et al., 2002)			NOAA/GMD sun-photometers (Dutton et al., 2004; Stone, 2002)	
	SP1A model	SP2H model	STAR01 model	SP02 Carter Scott model	SP022 Carter Scott model
Spectral range (nm)	351–1062	367–1045	390–1050	411–862	368–1050
Number of channels	17	14	10	4	4
Peak wavelengths (nm)	351, **371**, **380**, **416**, 443, **500**, 532, **609**, **675**, **778**, **864**, 911, (947), (961), **1025**, 1046, 1062	367, **380**, **413**, 441, **501**, 531, **605**, **673**, **776**, **862**, (912), (949), **1023**, 1045	390, 441, 501, 531, 605, 673, 776, 862, (949), 1045	412, 500, 675, 862	368, 610, 778, 1050
Full-width-half-maximum FWHM (nm)	3–10	3–10	3–15	10	10 (5 at 368 nm)
Entrance optical system	Quartz window	Quartz window	Telescope Maksutov (180 mm/1800 mm)	Quartz window	Quartz window
Aperture diameter (mm)	10	10	1	4	4
Angular Field of View (FOV) diameter	1°	1°	1°	5°	5°
Detector	Photodiode Hamamatsu S 1337 − 66BQ	Photodiode Hamamatsu S 1337 − 66BQ	Avalanche diode SQ37	UV Si-photodiode	UV Si-photodiode
Detection area (mm^2)	4	4	0.1	32	32
Operating temperature	−40 °C to +30 °C	−40 °C to +30 °C	−30 °C to +15 °C	−50 °C to +70 °C[a]	−50 °C to +70 °C[a]
Thermal control	Temperature shift is taken into account using appropriate temperature coefficients throughout the operative temperature range		30.0–30.5 °C	±1 °C of set point	±1 °C of set point
Accuracy of the AOD measurements	0.005–0.008	0.005–0.008	0.005–0.008	0.005	0.05 (at 610 and 778 nm); 0.01 (at 368 and 1050 nm)

[a] Minimum operating range is extended via thermal control to about −50 °C ambient temperature.

same approach used by Tomasi et al. (2007), this summer-time analysis ignores influences of AH and/or Asian dust (AD) that occur mainly during late winter and spring (Rahn et al., 1977; Shaw, 1982, 1983; VanCuren and Cahill, 2002; Stone et al., 2007; Quinn et al., 2007).

Tomasi et al. (2007) showed that the summer BG aerosol cases are distinguishable in terms of AOD from signatures of AH, AD and FFS events: the values of AOD(500 nm) measured for AH, AD and FFS cases in general exceed 0.10 and are appreciably lower under typical background conditions, while exponent α can assume values varying over the range between about 0.5 and 2.0 and are sometimes difficult to use to distinguish aerosol types, although Stone (2002) and Treffeisen et al. (2007) suggested spectral signatures of AOD useful for identifying different types of Arctic aerosol. Here, selection criteria for distinguishing the BG aerosol from AH, AD or FFS episodes are based solely on the examination of AOD(500 nm) using a threshold of < 0.08: details are described in the following sections.

2.1. Time series of AOD at Ny-Ålesund (Spitsbergen, Svalbard)

The first data-set examined in the present study consists of all the spectral series of AOD measured at Ny-Ålesund (78° 54′ N, 11° 53′ E, 2 m a.m.s.l., Koldewey-AWIPEV station) by the AWI group from March 1991 to September 2010. The data-set includes the AOD measurements performed from 1991 to spring 2006, and the more recent measurements performed from May 2006 to September 2010. All the AWI data were recorded using the SP1A and SP2H sun-photometers and the STAR01 star-photometer having the specific characteristics listed in Table 1 (Herber et al., 2002).

A supplementary data-set recorded in the Svalbard area was considered for comparison with the AWI data, consisting of the daily spectral series of AOD measured at Hornsund (77° 00′ N, 15° 33′ E, 10 m a.m.s.l.) (Polish Academy of Sciences), on Polar Bear Bay (Spitsbergen), from April 2005 to September 2009. Level 2.0 data were downloaded from the AERONET (Holben et al., 1998) website (http://aeronet.gsfc.nasa.gov/), derived from measurements made using a Cimel CE-318 sun-photometer (Table 2).

All the AWI spectral data were then analyzed using the best-fit procedure based on the well-known Ångström's (1964) formula to determine the pair of atmospheric turbidity parameters α and β for each AOD spectrum (Herber et al., 1993, 2002). Fig. 1 presents some examples of this best-fit procedure applied to spectral series of AOD measured with the SP1A and SP2H sun-photometers for different atmospheric turbidity conditions observed on summer clear-sky days representing BG aerosol conditions, and during AH episodes typical of the winter–spring period. The examples show that the best-fit values of α and β were obtained for regression coefficients better in general than −0.96 over the 416–864 nm and the 413–862 nm wavelength intervals chosen for the SP1A and SP2H sun-photometers, respectively. All daily sets of AOD measurements recorded at Ny-Ålesund by the AWI group were then examined to determine the daily mean values of AOD(500 nm) and α over a 20-year period from March 1991 to September 2010. The time series of AOD and α are shown in Fig. 2, compared with similar time series derived from the Level 2.0 AERONET data recorded at

Table 2
Main instrumental characteristics of the two sun-photometers employed by the IAO-SB group (Tomsk, Russia) and the AERONET team at Tiksi in summer 2010. The peak wavelengths in bold characters refer to the narrow-band interference filters used to determine the spectral values of AOD, while the peak wavelengths in brackets are those used to measure precipitable water.

Instrumental characteristics	Instruments	
	IAO-SB sun-photometer (Sakerin et al., 2009) Portable SPM	AERONET sun-photometer (Holben et al., 1998) CIMEL CE-318
Spectral range (nm)	340–2140	340–1020
Number of channels	12	8
Peak wavelengths (nm)	**340**, **379**, **443**, **499**, **548**, **676**, **871**, (941), **1019**, 1244, 1555, 2134	340, 380, **440**, **500**, **675**, **870**, (940), **1020**
Full-width-half-maximum, FWHM (nm)	3 (at 340 and 379 nm)–13 (at 2134 nm)	3 (at 340 and 380 nm)–10 (at the 440–1020 nm wavelengths)
Entrance optical system	Quartz window	Quartz window
Angular field of view (FOV) diameter	2.2°–3° (from 340 to 1019 nm); 3.2°–4.4° (from 1244 to 2134 nm)	1.2°
Detector	Si photodiode FDUK-13 (340–1020 nm); InGaAs photodiode Hamamatsu G 8373 (1200–2200 nm)	Silicon detector Hamamatsu (model S1336)
Operating temperature	Ambient temperature	−30 °C to +60 °C
Thermal control	Use of a thermostating system providing a stable internal temperature of 25 °C ± 0.5 °C.	Use of a thermistor measuring the temperature of the detector allowing compensation for any temperature dependence in the silicon detector
Accuracy of the AOD measurements	0.01–0.02	0.01–0.02

Hornsund, where the values of α have been calculated over the 440–870 nm wavelength range to be consistent with the AWI measurements. Two features are clearly evident in Fig. 2: (i) the regular sequence of AOD peaks in the winter–spring periods due to frequent Arctic Haze (AH) episodes, and (ii) the high values of AOD associated with relatively low values of α during the periods characterized by the presence of stratospheric loadings of ageing volcanic aerosols. The two features were analyzed for purposes of (a) characterizing the AH spectral extinction properties, and (b) removing the volcanic particle extinction effects in order to better define the typical summer BG aerosol extinction features.

2.1.1. Arctic haze characterization

Fig. 2 shows that the daily mean values of AOD(500 nm) varied mainly between 0.12 and 0.25 during the winter–spring periods, as

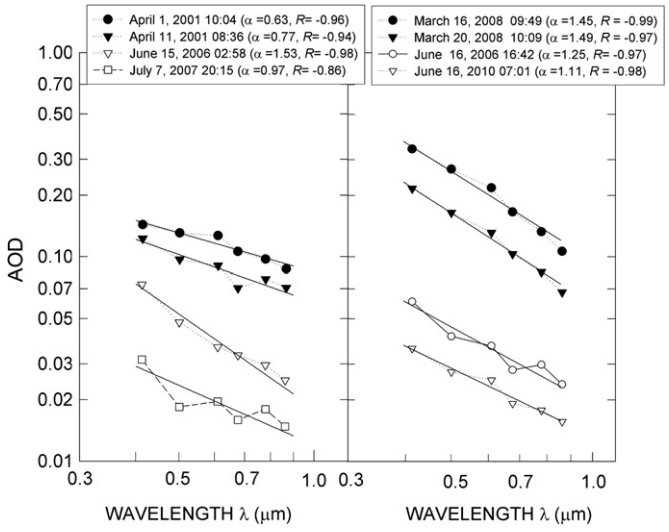

Fig. 1. Application examples of the best-fit procedure based on the Ångström (1964) formula to eight spectral series of AOD measured at the Ny-Ålesund (Koldewey/AWIPEV) station, using the SP1A (left) and SP2H (right) sun-photometers (see Table 1) on summer clean-air days (open symbols) and winter–spring days in the presence of Arctic haze (solid symbols). The best-fit values of Ångström's exponent α calculated for the spectral series of AOD measured on different days are given together with the corresponding values of regression coefficient R, as obtained over the 416–864 nm and the 413–862 nm wavelength intervals for the SP1A and SP2H sun-photometer models, respectively.

a result of the numerous AH transport events. To better evaluate the effects due to AH and separate the summer BG cases from the FFS ones, the relative frequency histograms of AOD(500 nm) were calculated separately by examining the daily mean values of this optical parameter for the June–September and December–May periods, excluding the periods in which strong extinction effects were caused by stratospheric volcanic particle layers. The results are presented in Fig. 3, where the summer histogram exhibits a maximum higher than 20% at AOD(500 nm) = 0.045 and presents a sharp left wing with 50% half-width centred at AOD(500 nm) = 0.030 and 10% half-width at AOD(500 nm) = 0.02. The right wing is long-tailed, presumably as a result of the frequent FFS transport episodes from North America and Siberia. It can be noted in Fig. 3 that the Gaussian curve centred at AOD(500 nm) = 0.045 shows (i) a right wing with 10% half-width at AOD(500 nm) = 0.08, giving a statistical indication that the summer BG values of AOD(500 nm) should all be smaller than 0.08, and (ii) a long-tailed right wing, which is presumably given by the relatively high number of FFS particle transport episodes occurring in the Svalbard region. The estimate of a threshold value of 0.08 for the BG aerosol cases agrees very well with the evaluations of AOD(532 nm) performed by Herber et al. (2002), who found a mean summer value of AOD = 0.046 ± 0.012 at this wavelength, with more than 90% of the AOD(532 nm) measurements ranging between 0.022 and 0.070 during summer. On the basis of these evaluations, it was decided to assume a threshold value of 0.08 to distinguish the summer BG values of AOD(500 nm) from the summer values affected by FFS extinction. The correctness of this assumption is confirmed by the shape of the relative frequency histogram reported in Fig. 3 for the winter–spring cases, which presents a long-tailed right wing over the range AOD > 0.08, due to the relatively high occurrence of AH episodes, and a left wing characterized by an evident flex at AOD(500 nm) = 0.065, produced by the overlap of a mode including the winter clean-air cases on a mode of higher AOD values arising from the numerous AH cases. Thus, the above threshold value of 0.08 is suitable for separating the winter clean-air cases from the AH ones also at other Arctic sites.

2.1.2. Adjustment of the volcanic particle extinction effects

In order to evaluate only summer BG values of AOD at Ny-Ålesund, steps were also taken to eliminate the effects of volcanic aerosols that are episodically present in the Arctic, as follows:

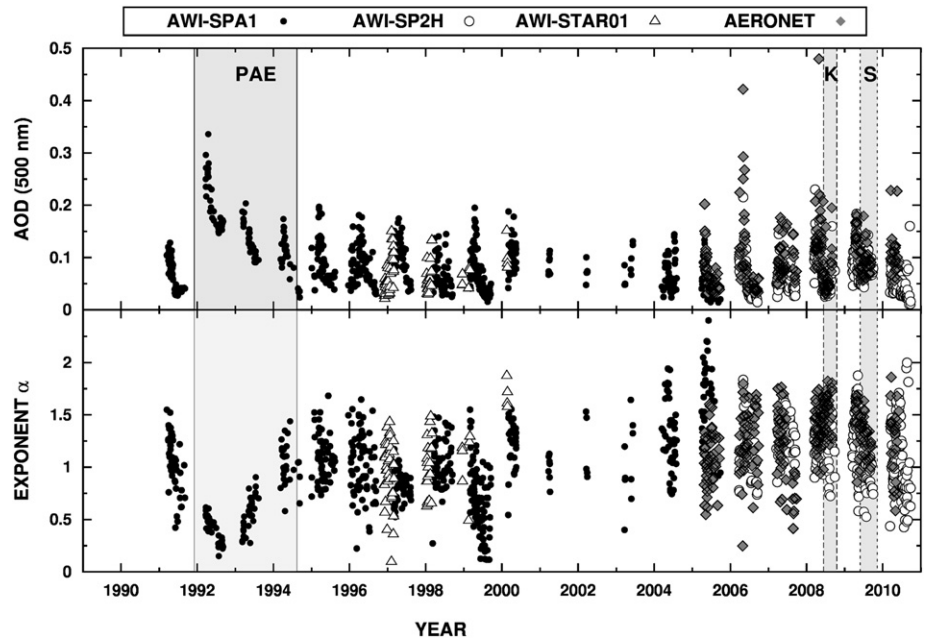

Fig. 2. Time series of the daily mean values of aerosol optical depth AOD(500 nm) (upper part) and Ångström's (1964) exponent α (lower part), as obtained from the measurements performed by the AWI group at the Ny-Ålesund (AWIPEV) station (Spitsbergen, Svalbard, Norway) from 1991 to 2010, using the SP1A (solid circles) and SP2H (open circles) sun-photometers, and the STAR01 star-photometer (open triangles). The time series of the daily mean values of AOD(500 nm) derived from the Level 2.0 AERONET measurements performed at Hornsund (grey diamonds) from April 2005 to September 2009 are also shown for comparison. The 3-year period from 1992 to 1994, when the AOD(500 nm) and α measurements were strongly affected by the Pinatubo particle extinction effects (PAE), is indicated by the grey vertical band. Similarly, the summer periods of 2008 and 2009 are marked by two narrow grey vertical bands labelled with letters K and S to indicate the data affected by extinction effects produced by the Kasatochi and Sarychev volcanic particle loadings, respectively.

(1) The entire 1991–2010 data-set was first examined following the same procedure used by Tomasi et al. (2007) by (i) assuming that the decay time of Pinatubo stratospheric aerosol particles was about 2–3 years on the basis of analysis by Stone et al. (1993), thus omitting data recorded during the 1992–1994 period; and (ii) calculating the monthly mean values of AOD(500 nm) and exponent α without excluding the data affected by FFS particle extinction. The monthly mean values of AOD obtained for the summer months were then plotted in Fig. 4 as a function of time over the entire period,

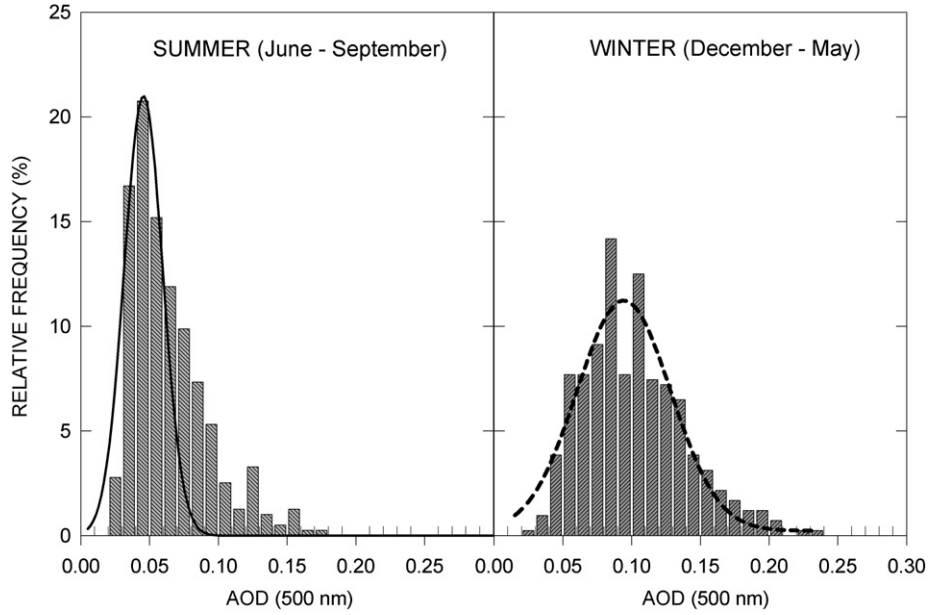

Fig. 3. Relative frequency histograms of AOD(500 nm) obtained by examining the set of AWI sun-photometer measurements performed at Ny-Ålesund from 1991 to 2010, from which the data affected by Pinatubo particle extinction during the 1992–1994 period have been omitted. The left part shows the histogram of the measurements performed on summer days from June to September, for which the best-fit Gaussian (solid) curve was found with maximum equal to 20.8% at AOD = 0.045 and standard deviation $\sigma = 0.015$. The right part shows the histogram obtained for the AOD measurements performed on winter–spring days (December–May) mainly characterized by AH conditions, for which the best-fit Gaussian (dashed) curve shown in the right part was obtained, with maximum equal to 11.0% at AOD(500 nm) = 0.0944, and $\sigma = 0.820$.

finding a regression line with a slightly negative slope coefficient $k = -0.021\%\ y^{-1}$. These results show an appreciable change in the magnitude of the long-term variation in summer BG values of AOD with respect to the value of $k = -2.2\%\ y^{-1}$ found by Tomasi et al. (2007) for the 1991–2006 period. The new result suggests that the extinction by enhanced stratospheric loading of volcanic particles may have contributed to the change represented by the slope parameter k. There is evidence, on the global scale, of slowly increasing stratospheric AOD over the last decade as a result of minor volcanic eruptions (Solomon et al., 2011).

(2) The dominant effects of volcanic particles were removed in the second step, including those from (i) the Pinatubo eruption (15° 08′ N, 120° 21′ E) on June 15, 1991, (ii) the Kasatochi (52° 10′ N, 175° 31′ W) eruption of August 7 and 8, 2008, and (iii) the Sarychev (48° 06′ N, 153° 12′ E) eruption of June 12, 2009. The daily mean values of total atmospheric AOD were adjusted to account for these stratospheric volcanic aerosol effects as follows: (a) the adjustment of the Pinatubo measurements of AOD was made using the SAGE II estimates of stratospheric AOD(532 nm) given by Herber et al. (2002) for the 1992–1996 period, which indicated that volcanic AOD decreased at Ny-Ålesund from about 0.16 in the early months of 1992 to less than 0.01 in October 1996; and (b) the daily mean values of total atmospheric AOD(500 nm) measured with the AWI sun-photometers from August 15 to September 27, 2008, and those measured from July 3 to early October, 2009, were adjusted for the Kasatochi and Sarychev volcanic particle extinction effects, respectively, by subtracting the values of stratospheric AOD(500 nm) derived from the vertical profiles of aerosol extinction coefficient at the 532 nm wavelength measured with the Koldewey Aerosol Raman Lidar (KARL) by Hoffmann et al. (2010) during summer 2008, and Hoffmann (2010) during summer 2009 (see also O'Neill et al., 2012). For the adjusted values of monthly mean AOD the slope coefficient k was evaluated to be slightly positive and equal to $+0.006\%\ y^{-1}$, which still includes the extinction effects due to the frequent summer FFS episodes.

(3) In the third step, the summer BG values of AOD were selected to exclude the data measured on days characterized by the presence of significant loadings of FFS particles. Using the threshold value of 0.08 determined in Fig. 3, the daily mean values of AOD(500 nm) associated with summer BG aerosol conditions were selected by rejecting days having AOD(500 nm) > 0.08. Fig. 4 shows the time series of monthly mean BG values of AOD(500 nm) recorded by AWI during the summer season, with essentially a null slope coefficient ($k = -0.01\%\ y^{-1}$).

The long-term average variation in AOD(500 nm) was also calculated for the set of monthly mean values of AOD(500 nm) determined in the summer months at the Hornsund AERONET site from April 2005 to September 2009. Omitting the monthly mean values of AOD(500 nm) affected by the Kasatochi and Sarychev particle extinction, a best-fit value of $k = +1.0\%\ y^{-1}$ was found. Therefore, the daily mean values of AOD were first adjusted for the stratospheric volcanic AOD due to the Kasatochi and Sarychev volcanic particles present in the stratosphere during the summer months of 2008 and 2009, respectively: the daily values of stratospheric AOD were determined according to the monthly mean estimates of this quantity obtained by Kravitz et al. (2010) for Kasatochi eruption, and by Kravitz et al. (2011) and Haywood et al. (2010) for Sarychev episode, on the basis of both satellite-borne observations and climate model simulations. For such adjusted monthly mean values of AOD, a lower value of $k = +0.4\%\ y^{-1}$ was found. The daily residual values of AOD were then examined rejecting the values of AOD(500 nm) > 0.08, which are probably associated with the presence of FFS loadings, and subsequently

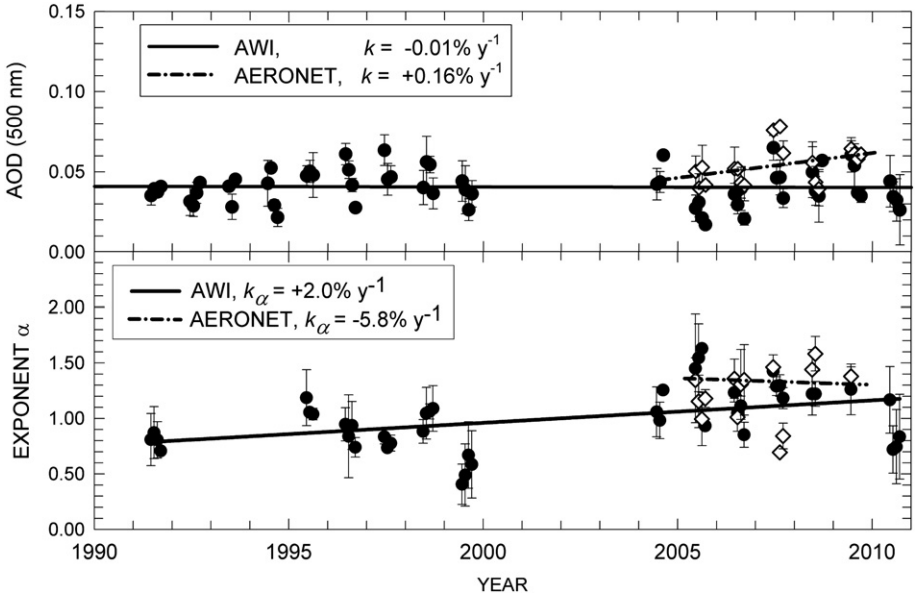

Fig. 4. Time series of the monthly mean values of AOD(500 nm) (upper part) and Ångström's exponent α (lower part) obtained as averages of the daily mean values of the two optical parameters (solid circles) derived from the AWI sun-photometer measurements performed at Ny-Ålesund with the SP1A and SP2H sun-photometers and STAR01 star-photometer. The time-patterns of the monthly mean values of AOD(500 nm) and α obtained from the AERONET sun-photometer measurements performed at Hornsund (open diamonds) are also given for comparison. For all the data-sets, the vertical bars define the standard deviations. The best-fit regression lines drawn for the AWI AOD (solid line) and AERONET AOD (dashed and dotted line) data-sets are shown giving best-fit values of slope coefficient $k = -0.01\%\ y^{-1}$ and $k = +0.16\%\ y^{-1}$, respectively. A value of relative slope coefficient $k_\alpha = +2.0\%\ y^{-1}$ of the regression line was found in the lower part, indicating that a weak increase in α was observed over the period from 1991 to 2010, presumably due to the increasing contribution of anthropogenic aerosols. The value of $k_\alpha = -5.8\%\ y^{-1}$ determined at Hornsund over the 2005–2009 period is less significant because of the shorter (5-year) observation period.

subdivided into monthly sets for which the monthly averages were calculated, obtaining a best-fit line with a slightly positive value of $k = +0.16\%\ y^{-1}$, which can be reasonably explained as due to a major contribution of anthropogenic aerosol particles transported from European polluted areas. The results given in Fig. 4 also show that the negative value of k found by Tomasi et al. (2007) was at least in part due to the omitted adjustment for volcanic particle extinction effects during the decay phase in 1995 and 1996, and the occurrence of relatively high values of AOD(500 nm) from 1997 to 2000.

The monthly mean values of exponent α were correspondingly calculated for all the measurements performed on summer days to assess BG aerosol characteristics, by excluding periods affected by Pinatubo, Kasatochi and Sarychev volcanic eruptions. Therefore, the monthly mean values of exponent α presented in Fig. 4 can be correctly attributed to BG aerosol conditions measured at Ny-Ålesund (1991–2010), and show a significant increase with mean slope coefficient $k_\alpha = +2.0\%\ y^{-1}$, which may be due to an increase in the anthropogenic contribution from mid-latitudes in recent decades. The Hornsund values of α differ markedly from those obtained at Ny-Ålesund: however, the regression considers only five years of data in which is $k_\alpha = -5.8\%\ y^{-1}$.

2.2. Time series of AOD at Barrow (Alaska)

An important part of the Arctic AOD data analyzed in the present paper was derived from the measurements routinely performed at Barrow (71° 19′ N, 156° 36′ W, 8 m a.m.s.l.) by the NOAA/GMD group from April 1977 to August 2010, using the Filter Wheel Normal Incidence Pyrheliometer (FWNIP). Examining this multi-year series of FWNIP measurements, a long series of daily mean values of mean visible AOD_{FWNIP} was obtained. Therefore, the present Barrow data-set includes all the daily mean values of AOD_{FWNIP} previously analyzed by Tomasi et al. (2007) and those measured with the same technique during the subsequent 10 years, April 2001–August 2010. In addition, a large set of sun-photometer measurements recorded over the period from February 2002 to October 2010 was examined in the present study to determine the time series of AOD(500 nm) and exponent α from the daily sets of spectral values of AOD measured by the NOAA/GMD group using the SP02 and SP022 Carter Scott sun-photometers at the wavelengths listed in Table 1 (Stone, 2002). To better characterize the atmospheric turbidity conditions at Barrow, we also examined the time series of AERONET Level 2.0 AOD(500 nm) data recorded within six spectral channels centred at wavelengths ranging between 340 and 1020 nm, June 1999–August 2010.

Fig. 5 shows the time series of the daily mean values of AOD_{FWNIP}, those of AOD(500 nm) obtained with the SP02 and SP022 sun-photometers, and the AOD(500 nm) measured by AERONET for April 1977–October 2010. Especially high values were obtained during all the volcanic periods and seasonally during occurrences of AH and FFS. Fig. 5 also presents the record of α derived using (i) the FWNIP measurements following the procedure of Bernhard et al. (2007); (ii) the spectral series of AOD determined from the SP02 and SP022 sun-photometer measurements (Table 1), applying the Ångström (1964) best-fit method described above (Fig. 1); and (iii) the AERONET Level 2.0 estimates of α determined over the 440–879 nm spectral range (1999–2010). It should be pointed out that the AOD_{FWNIP} measurements have a lower accuracy than the values of AOD(500 nm) directly measured with the SP02 and Cimel sun-photometers (Dutton et al., 2004). Comparing the measurements of AOD_{FWNIP} with those of AOD(500 nm) directly obtained from the Cimel sun-photometer

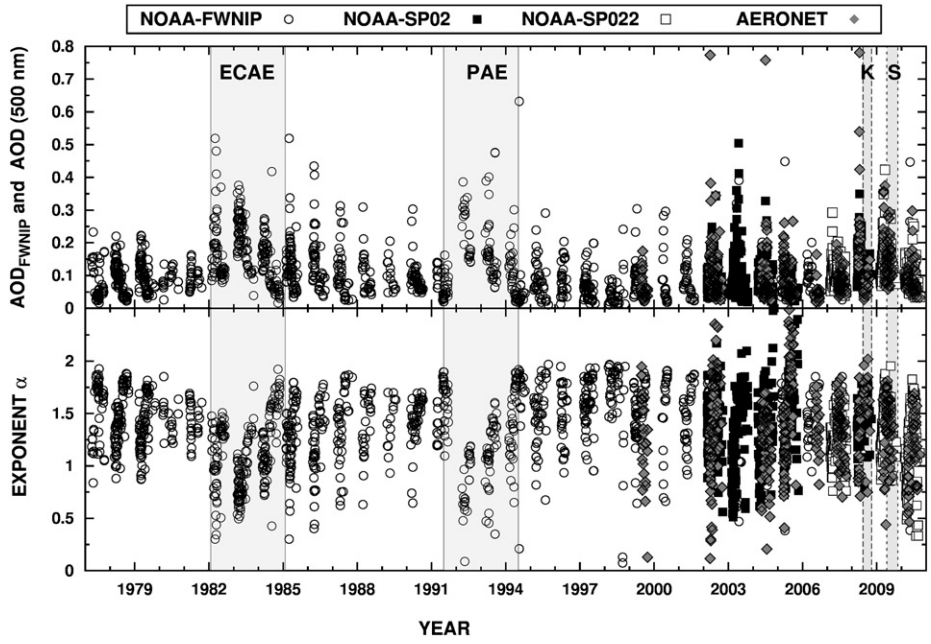

Fig. 5. Time series of the daily mean values of aerosol optical depth AOD_{FWNIP} (upper part) and Ångström's (1964) exponent α (lower part): AOD_{FWNIP} was obtained from the routine measurements performed at Barrow (Alaska) by the NOAA/GMD group using the Filter Wheel Normal Incidence Pyrheliometer (FWNIP) (open circles) over the 34-year period from April 1977 to August 2010, while exponent α was evaluated using the algorithm of Bernhard et al. (2007). The two FWNIP series of AOD and α are compared with (1) those of AOD(500 nm) derived from the SP02 Carter Scott sun-photometer measurements (solid squares), (2) those of α determined from the overall set of SP02 (solid squares) and SP022 sun-photometer (open squares) measurements, as performed by the NOAA/GMD group during the 9-year period from February 2002 to October 2010; and (3) those determined from the Level 2.0 AERONET sun-photometer measurements performed at Barrow over the 12-year period from June 1999 to September 2010 (grey diamonds). The measurements recorded during the 1982–1984 and 1992–1994 periods for strong stratospheric particle extinction due to the El Chichón and Pinatubo volcanic eruptions are evidenced by the grey vertical bands labelled ECAE and PAE, respectively. Similarly, the summer periods of 2008 and 2009, in which marked volcanic particle extinction effects were observed due to the Kasatochi and Sarychev eruptions are marked by two narrow grey vertical bands labelled with letters K and S, respectively.

measurements recorded at Barrow, Bernhard et al. (2007) found a very good correlation between the AOD_{FWNIP} and AOD(500 nm) values, defined for an overall regression coefficient $R = +0.91$. To verify the reliability of the present estimates of AOD_{FWNIP} and evaluate their consistency with the AOD(500 nm) evaluations derived from the SP02 sun-photometer measurements, Fig. 6 presents a comparison between the daily mean FWNIP values of AOD determined on 149 days during the period from February 2002 to October 2010 and the coincident daily mean SP02 values of AOD(500 nm). There is a fair correlation between these two time series with intercept very close to null and a slope coefficient not far from unity. Discrepancies are attributed mostly to the uncertainty in evaluating AOD_{FWNIP} and also infrequent sampling using the FWNIP compared with SP02s that record values every minute of the day when cloud-free.

It is evident in Fig. 5 that daily mean measurements of AOD performed at Barrow, and α inferred from them using the Bernhard et al. (2007) algorithm, for the 1982–1984 and 1992–1994 periods, are strongly affected by the stratospheric particle extinction due to the El Chichón and Pinatubo volcanic eruptions (Dutton and Christy, 1992; Stone et al., 1993) occurring in March–April 1982 and June 1991, respectively. In order to distinguish the effects produced by such volcanic particles and from those due to biomass burning and FFS pollution episodes in the summer months, the procedure adopted to analyze Ny-Ålesund data was also applied to the Barrow data-set described above, as follows:

(1) The AOD_{FWNIP} and AOD(500 nm) data were examined separately, imposing the same criteria as Tomasi et al. (2007). The AOD data recorded during the 1982–1984 and 1992–1994 periods and in the summer periods of 2008 and 2009 were first omitted to exclude the volcanic contributions. Subsequently, the monthly mean values of AOD and α were determined for the summer months, including the FFS data. The FWNIP time series of AOD was fitted linearly to obtain slope coefficient $k = +0.001\%\ y^{-1}$. A similar analysis of the SP02 data gave a value of $k = +0.03\%\ y^{-1}$. The combined analysis, which shows increases in both AOD_{FWNIP} and AOD(500 nm) at Barrow over the past 6–8 years, indicates a reversal of the trend noted by Tomasi et al. (2007) with $k = -1.6\%\ y^{-1}$).

(2) In the second step, the AOD data affected by volcanic particle extinction were adjusted for periods affected by El Chichón and Pinatubo and also by minor eruptions of Okmok, Kasatochi, Mt. Redoubt and Sarychev during 2008 and 2009. The adjustments of AOD_{FWNIP} data were made on the basis of anomalies determined by Dutton and Christy (1992) for a period from spring 1982 to the end of 1984. The values of volcanic AOD generated by the Pinatubo eruption were calculated taking into account the evaluations of Dutton and Christy (1992) for 1992 and those of Stone (2002) for the period from spring 1992 to late 1996. Similarly, the adjustment of the monthly mean values of AOD obtained in the summer months of 2008 and 2009 (for the above-mentioned four eruptions) was done using the estimates of stratospheric AOD provided by Kravitz et al. (2010) for the Okmok and Kasatochi volcanic effects, and by Haywood et al. (2010), Kravitz et al. (2011), and O'Neill et al. (2012) for the Mt. Redoubt and Sarychev effects, respectively.

Examining the time series of the monthly mean values of AOD_{FWNIP} (summer only) for 1977–2010, including both BG and FFS values of AOD, we obtained slope coefficient $k = -0.002\%\ y^{-1}$, which is no measurable change when removing contributions from volcanic aerosols. Analysis of the time series of monthly mean values of AOD(500 nm), determined with SP02 sun-photometers over the 2002–2010 period, provided a value of $k = -0.09\%\ y^{-1}$, indicating some decrease in AOD for the BG + FFS particles.

(3) Finally, a selection of pure summer BG values of AOD was made by rejecting FFS events and re-fitting the time series, assuming the threshold BG value of 0.08 (Fig. 3). Results are presented in Fig. 7 for the period, 1977–2010. The following regression slopes were computed:
   (i) a nearly null value, $k = -0.02\%\ y^{-1}$, for the AOD_{FWNIP} data only;
   (ii) a slightly negative value of $k = -0.05\%\ y^{-1}$ for SP02 data only; and
   (iii) $k = +0.06\%\ y^{-1}$ for the overall set of AERONET Level 2.0 values of AOD, showing that the AERONET result obtained for 1997–2010 does not differ appreciably from that given by the SP02 measurements over the last 9 years.

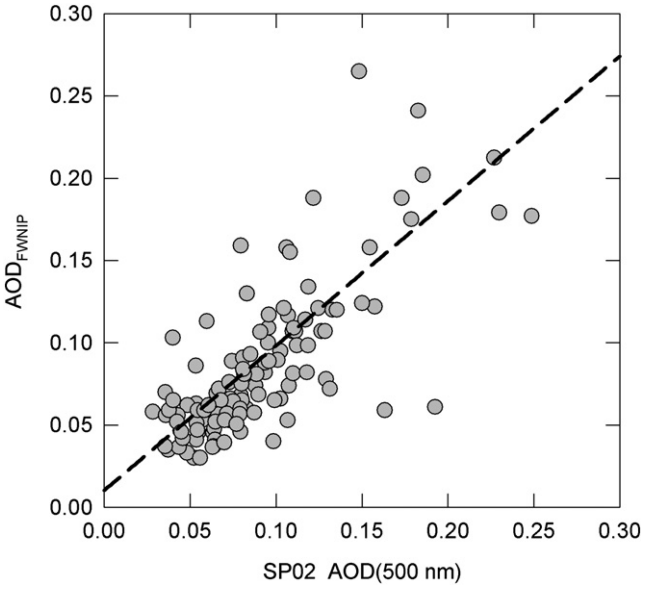

Fig. 6. Scatter plot of the daily mean values of AOD_{FWNIP} derived from the Filter Wheel Normal Incidence Pyrheliometer measurements performed at Barrow by the NOAA/GMD group from February 2002 to October 2010 versus the simultaneous daily mean values of AOD(500 nm) obtained from the SP02 sun-photometer measurements. The best-fit dashed line was determined for a total number of 149 cases, with intercept equal to 0.01, slope coefficient equal to +0.88 and regression coefficient $R = +0.58$.

The results obtained examining the updated time series of AOD over the 1977–2010 period indicate that a change has occurred in the long-term average slope of this optical parameter, mainly due to the rather high values measured during the past decade, passing from a negative value of $-1.6\%\ y^{-1}$ over the 26-year period from 1977 to 2002 to values very close to null over the last 10 years. Because the present analysis refers to summer BG aerosols only, it is important to highlight that this change in the AOD slope coefficient cannot be attributed to events, such as volcanic eruptions, AH occurrence or FFS transport episodes, but rather to a slowly increasing contribution due to background aerosol extinction presumably caused by the recently increasing emissions of pollutants in the mid-latitude areas of the Northern hemisphere. This explanation is consistent with the increase in anthropogenic emissions reported by Hirdman et al. (2010). They performed a cluster analysis of model output from the Lagrangian particle dispersion model, FLEXPART (Stohl et al., 1998), run backward in time, relative to Alert, Barrow and Zeppelin (Ny-Ålesund). Their results indicate that equivalent black carbon (EBC) and sulphate concentrations are mainly associated with transport from Northern

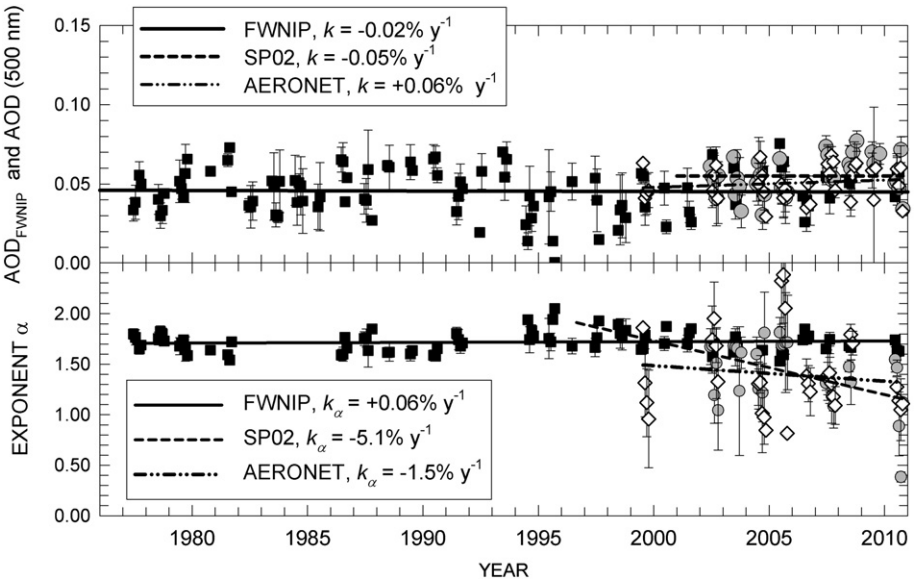

Fig. 7. Time series of the monthly mean values of aerosol optical depth AOD_{FWNIP} and AOD(500 nm) (upper part) and exponent α (lower part) obtained by averaging the daily mean values of the two optical parameters (solid squares). The AOD_{FWNIP} values are derived from the FWNIP measurements performed at Barrow (Alaska) by the NOAA/GMD group over the 34-year period from April 1977 to August 2010, and those of α using the algorithm of Bernhard et al. (2007) applied to FWNIP data. The time series of monthly mean values of AOD_{FWNIP} and α are compared with (1) those obtained from the SP02 and SP022 sun-photometer measurements (grey circles) performed by the NOAA/GMD group from February 2002 to October 2010, and (2) those obtained from the Level 2.0 AERONET sun-photometer measurements performed at Barrow from June 1999 to August 2010 (open diamonds). The values of slope coefficient k giving the percentage long-term average variation of AOD per year and defined by the best-fit regression lines drawn for the FWNIP (solid line), SP02 (dashed line), and AERONET (dashed and dotted line) data-sets are given in the upper graph, while the best-fit regression lines shown in the lower graph with different values of slope coefficient k_α provide evidence of the marked decrease of α observed over the past 9 years.

Eurasia, which was identified as the dominant emission source over the past decade at all Arctic stations for EBC. Another possible contributing factor is increasing emissions from coal burning in China during the recent decade. An appreciable increase in the sulphate aerosol loading at mid-latitudes, followed by dispersion within the stratosphere was hypothesized by Hofmann et al. (2009). The subsequent transport of these particles into the Arctic stratosphere has also been suggested (Vernier et al., 2009; Stone et al., 2010).

Fig. 7 also shows the monthly mean values of α for 1977–2010, calculated for BG conditions only. An appreciable decrease in α is noted during the past decade, as determined from the NOAA SP02/SP022 data, yielding $k_\alpha = -5.1\%\ y^{-1}$, while analysis of AERONET data has produced a value of $k_\alpha = -1.5\%\ y^{-1}$ for period, 1999–2010. The marked decreases in α are likely due to a relative increase in the concentration of large sulphate particles of anthropogenic origin, as suggested by Hirdman et al. (2010). Another possible contributor is the increasing burden of ageing stratospheric aerosol from minor volcanic eruptions that have added to the BG. For instance, particle formation following the eruption of the Soufrière Hills (16° 43′ N, 62° 11′ W) volcano in May 2006 (Prata et al., 2007) may have been dispersed poleward via upper-level transport (Vernier et al., 2009).

2.3. Time series of AOD at the Arctic Siberian sites

Long-term measurements of AOD were performed by the AARI group (Arctic and Antarctic Research Institute, St. Petersburg, Russia) during the 11 years from 1981 to 1991 at the Siberian stations of Dikson Island (76° 30′ N, 87° 54′ E, 12 m a.m.s.l.), Severnaya Zemlya (79° 00′ N, 100° 00′ E, 7 m a.m.s.l.), Kotel'ny Island (76° 00′ N, 137° 54′ E, 8 m a.m.s.l.), and Wrangel Island (71° 14′ N, 179° 36′ W, 10 m a.m.s.l.). The measurements were carried out using thermoelectric actinometers equipped with a set of glass bandpass filters, having short-wavelength cutoffs at the 0.38, 0.47, 0.53, 0.63 and 0.71 μm wavelengths. Analyzing these actinometric measurements, a multi-year set of monthly mean values of aerosol optical depth AOD_{act} was collected at a visible wavelength close to 500 nm (Radionov and Marshunova, 1992; Radionov, 2005). The AOD_{act} values were obtained from measurements performed in both clean-air and polluted-air conditions, from which Tomasi et al. (2007) found that AOD_{act} underwent a considerable decrease over the 1981–1991 period, with an average slope coefficient of $-7.6\%\ y^{-1}$, attributed to the sharply diminishing anthropogenic emissions of SO_2 in Europe and Russia, especially since 1985.

The time series of monthly mean AOD_{act} measured in summer at the above 4 Siberian sites are shown in Fig. 8, where the data obtained for the months predominantly characterized by BG aerosol conditions are examined separately from those with more polluted-air conditions, which are due to the arrival of air masses containing anthropogenic particulate matter from the Eurasia area and, to a lesser extent, FFS particulate matter from the Siberian interior. Considering only the summer BG values of AOD_{act}, a regression line was drawn for Dikson Island, Severnaya Zemlya and Kotel'ny Island, finding an average decrease from about 0.08 in 1984 to 0.05 in 1988, defined by $k = -0.24\%\ y^{-1}$. This estimate is considerably smaller than that found by Tomasi et al. (2007) for the overall BG + FFS data-set. No measurements have been performed by the AARI group since 1991. Thus, in order to obtain a measure of AOD(500 nm), as currently observed in the Siberian coastal area of the Arctic Ocean, the monthly mean values of AOD obtained from the summer BG aerosol data recorded at Tiksi (71° 35′ N, 128° 47′ E, 40 m a.m.s.l.) in the North Central Siberia were also considered, as determined in (i) June 2010 from the measurements performed with the portable SPM sun-photometer manufactured by Sakerin et al. (2009) at the Institute of Atmospheric Optics (Siberian Branch, Russian Academy of Sciences, Tomsk, Russia) (IAO-SB, RAS), and (ii) June–September 2010 from the AERONET Level 2.0 measurements carried out with the Cimel CE-318 sun-photometer. The technical characteristics of both instruments are given in

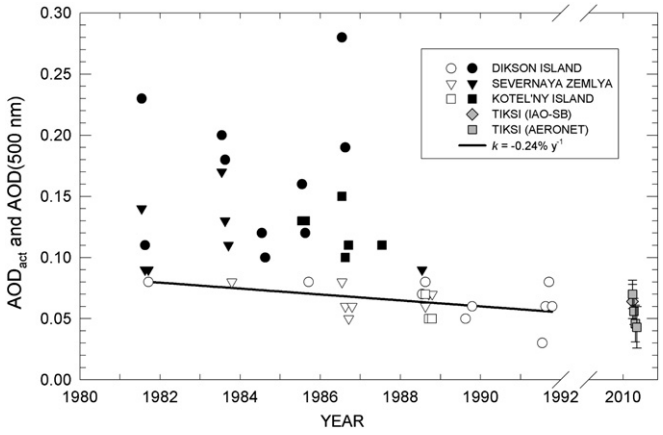

Fig. 8. Time series of the monthly mean values of aerosol optical depth AOD_{act} obtained from the measurements performed by the AARI group in the 1981–1991 summer months using multi-filtered thermoelectric actinometers at Dikson Island (circles), Severnaya Zemlya (triangles), and Kotel'ny Island (squares). The data were calculated as averages of the monthly sub-sets of daily mean values of AOD_{act} selected separately for BG aerosol conditions (open symbols) and polluted-air conditions (solid symbols). The regression line is drawn for the BG values of AOD_{act}, giving a best-fit slope coefficient $k = -0.24\%\ y^{-1}$. The BG aerosol data are compared with the monthly mean values of AOD(500 nm) obtained with their standard deviations (vertical bars) for the same atmospheric turbidity conditions from the SPM sun-photometer (grey diamond) measurements performed at Tiksi by the IAO-SB group in June 2010, and from the Level 2.0 AOD(500 nm) measurements (grey squares) performed at Tiksi by the AERONET/GSFC group over the June–September 2010 period, using a Cimel CE-318 sun-photometer.

Table 2. The monthly mean SPM and Cimel values of AOD(500 nm) that are lower than the above-assumed threshold value of 0.08 are shown in Fig. 8, together with their standard deviations. Although affected by large uncertainties, they result in practice to be comparable with the BG values of AOD observed by the AARI team in 1988–1991, proving that the average atmospheric transparency conditions of the summer Arctic atmosphere have been quite stable over the last two decades in the North Central Siberian coastal area. The monthly mean values of exponent α associated with BG aerosol conditions were found to range mainly between 0.9 and 1.9 at Tiksi, during summer 2010.

3. Long-term variations in frequency and intensity of Arctic haze episodes

Examining the surface aerosol scattering nephelometric measurements conducted at Barrow from May 1976 to late 1992 and the FWNIP measurements performed from 1977 to 1991, Bodhaine and Dutton (1993) found that both surface-level scattering coefficient and AOD reached a maximum in 1982 and then decreased gradually, as a consequence of the decrease in anthropogenic pollution emissions in Europe and the former Soviet Union. In fact, very high AH extinction features were observed in the '80s and early '90s, subsequently decreasing with the reduction of SO_2 emissions in the major industrial areas of the Northern hemisphere. Such strong pollution occurrences have long been a subject of considerable interest and concern, since their source was initially uncertain, attributed mainly to natural factors. Only more recently, they have been predominantly ascribed to the transport of polluted-air masses of industrial origin from North America, Europe and Asia, and biomass burning particles generated by agricultural activities and/or boreal forest fires. In view of increasing aerosol emissions in the Asian area, Quinn et al. (2007) pointed out that it is reasonable to expect a corresponding increase in the frequency and intensity of AH episodes within a few years. However, while emission rates certainly exert an influence on the distribution of haze, changes in atmospheric transport were also a relevant factor, because atmospheric circulation has undergone significant changes in the Arctic region over the last decades, leading to variations in atmospheric circulation patterns affecting cloudiness features, temperature conditions and snowfall frequency (Stone, 1997; Stone et al., 2002).

In order to update the data-set containing information on the AH aerosol optical depth, atmospheric turbidity conditions and frequency of such episodes, the present study re-examined the time series of the daily mean values of AOD shown in Figs. 2 and 5, as measured at Ny-Ålesund and Barrow over the 1991–2010 and 1977–2010 periods, respectively. In analyzing these data, it was taken into account that nearly all AH episodes are observed during the winter–spring period of each year, from December to May, these months being generally characterized by a sharp increase in AOD. In fact, AOD(500 nm) often exhibits peaks > 0.12 that are comparable to those usually measured at mid-latitude stations of the Northern continental areas. The transport of pollutants from the mid- to the high-latitudes, leading to the formation of AH, is favoured in winter–spring because atmosphere cleaning due to particle scavenging by precipitations is particularly weak during this seasonal period (Stone et al., 2002). Fig. 3 shows that the relative frequency histogram of AOD(500 nm) measured at Ny-Ålesund on winter–spring days exhibits a large bimodal maximum in the 0.08–0.12 range, with a long-tailed right wing extending up to values of more than 0.20. Therefore, assuming the threshold of 0.08 defined in Fig. 3 to distinguish the clean-air AOD values from those occurring in AH episodes, the winter–spring data presented in Figs. 2 and 5 were re-examined to determine the following parameters for the 6-month period of each year from December to May: (i) the average value of AOD for AH events only, as obtained from the AWI sun-photometer measurements at Ny-Ålesund, and the FWNIP and SP02 sun-photometer measurements at Barrow; (ii) the average value of exponent α evaluated during AH episodes; (iii) the overall number N_{AH} of the AH events; and (iv) the cumulative 6-month value of AOD(500 nm), obtained by summing all the daily mean values of this quantity measured during the 6-month period.

The results are presented in Fig. 9, showing that: (a) the long-term variation of the 6-month average value of AOD(500 nm) for the AH episodes is characterized by very low values of slope coefficient k_{AH} defined by the regression lines, equal to $+0.02\%\ y^{-1}$ at Ny-Ålesund, and $-0.04\%\ y^{-1}$ at Barrow, indicating that significant long-term variations of AH intensity have not been present over the last 35 years; (b) the 6-month average value of α associated with AH events increased at Ny-Ålesund by $+2.5\%\ y^{-1}$ on average, over the 1991–2010 period, and increased by less than $0.1\%\ y^{-1}$ at Barrow, showing that appreciable variations in the size-distribution of AH particles may have occurred in the last 20 years; (c) the overall number of AH episodes observed at Ny-Ålesund varied from more than 20 in the 1996–2000 period to less than 10 in the 2001–2007 period, while at Barrow it was higher than 40 from 1978 to 1986 and since 2002, but lower than 20 during the intermediate period, thus indicating that no long-term variations of AH frequency were recorded at the two Arctic sites; and (d) the cumulative AOD was also subject to large fluctuations at both Ny-Ålesund and Barrow, presenting maxima and minima that in practice coincide with those of N_{AH}. In particular, the time-patterns of this parameter were estimated to vary mainly between 0.5 and more than 3 at Ny-Ålesund, and between less than 1 and more than 8 at Barrow, providing evidence of a higher and more intense occurrence of AH episodes since 2002, which may be plausibly attributed to the recent increase in pollutant emissions in the Asian region (Hirdman et al., 2010).

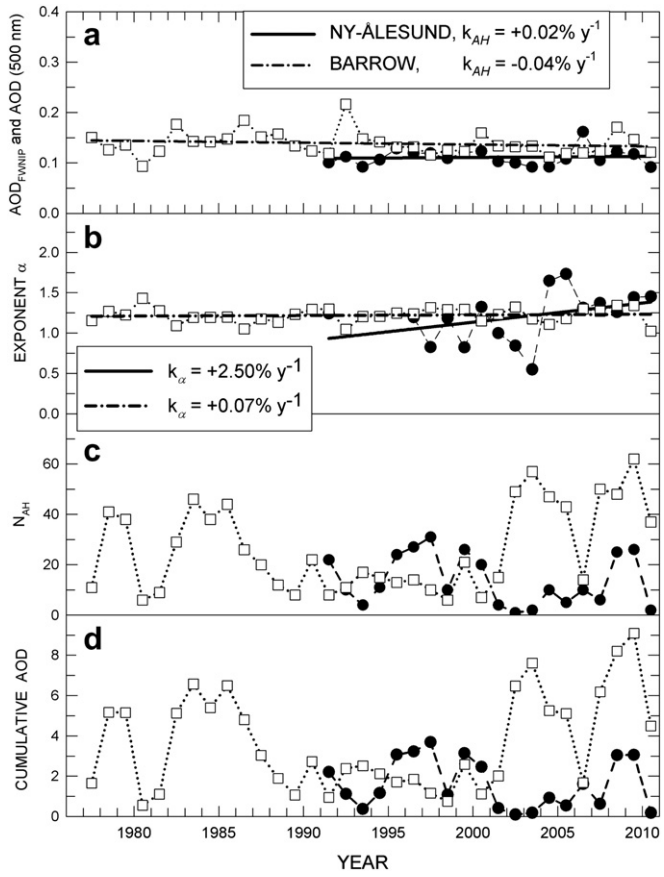

Fig. 9. Time series of the 6-month mean values determined at Ny-Ålesund and Barrow over the December–May period of each year for the following parameters: (a) AOD(500 nm), as derived from the AWI sun-photometer measurements performed at Ny-Ålesund (solid circles), and the (FWNIP + SP02 + SP022) measurement set at Barrow (open squares); (b) exponent α, as determined from the AWI sun-photometer at Ny-Ålesund and the (FWNIP + SP02 + SP022) data-set at Barrow; (c) overall number N_{AH} of the AH episodes recorded during each 6-month period; and (d) cumulative aerosol optical depth, AOD, obtained by summing all the AOD values recorded during the 6-month period and attributed to AH episodes.

4. Arctic aerosol radiative properties

The above evaluations of AOD and α for both summer BG aerosols and AH particles sampled in winter and spring can be used to obtain reliable evaluations of the direct aerosol-induced radiative forcing at TOA only knowing the chemical composition of particulate matter, from which the complex refractive index and the radiative properties of aerosol polydispersions can be derived. For this purpose, an evaluation of the mass fractions of the main particulate chemical components was performed, by taking into account the results found by Quinn et al. (2002), who examined a 3-year set of simultaneous measurements of aerosol chemical composition and light scattering and absorption measurements performed at Barrow from October 1997 to December 2000, for rather low relative humidity conditions. These estimates were given by Quinn et al. (2007) in terms of monthly mean concentrations of aerosol mass constituents, such as sea salt, non-sea salt (nss) sulphate, methane sulphonic acid (MSA), ammonium ions, and nss K, Mg and Ca ions, for both the submicron and supermicron size ranges. In the present study, the above data were integrated by (i) the estimates of total carbon (black carbon (BC) + organic carbon (OC)) concentration measured by Sharma et al. (2002, 2006) at Barrow, and (ii) the conversion from the above nss Mg and Ca ionic concentrations to the Al–Si components, using the soil factors proposed by Polissar et al. (1998) for the Northwest Alaska areas. For such features of particulate matter composition, the percentage mass fractions were determined for sulphates, nitrates, sea salt, mineral dust, water-soluble organic matter (WSOM) and BC components, in the submicron, supermicron and overall size-distributions, during the summer period from June to September, and for the rest of the year. The results are presented in Fig. 10.

The spectral patterns of the real part n_r and imaginary part n_i of the particulate refractive index were then calculated as weighted averages of the two optical parameters found for sulphates (Toon and Pollack, 1976), nitrates (Tang and Munkelwitz, 1996), sea salt (Shettle and Fenn, 1979), mineral dust (Dust-Like component of Vermote et al. (1997)), BC (Soot component of Vermote et al. (1997)), and WSOM (Water-Soluble component of Vermote et al. (1997)), using as weights the composition mass percentages given in Fig. 10 for the overall particle size-distributions sampled during the June–September (summer) and October–May (winter–spring) periods. The spectral patterns of parameters n_r and n_i are presented in Fig. 11, for both summer and winter–spring: it can be seen that the values of these optical parameters for winter–spring conditions are appreciably higher than those obtained in summer, mainly due to the higher sulphate concentration.

The values of ground-level single scattering albedo ω_o obtained for the above summer and winter–spring aerosol models were calculated following the same weighting procedure as for the mass fractions shown in Fig. 10. They are presented in Fig. 11 for the overall particle size-distribution and are compared with the evaluations of ω_o obtained by:

(a) Bodhaine (1995) at Barrow, examining a 6-year set of nephelometer and aethalometer measurements of the volume scattering and absorption coefficients at 550 nm wavelength, finding monthly median values that varied between 0.928 in March and 0.983 in January, with an annual median value of 0.958, thus describing an annual cycle providing an average winter value of 0.950 ± 0.018 and an average summer value of 0.974 ± 0.006;

(b) Heintzenberg et al. (1997), who obtained annual mean values of ω_o (550 nm) equal to 0.960 and 0.948 at Barrow and Ny-Ålesund, respectively;

(c) Delene and Ogren (2002), who obtained at Barrow a pair of annual mean values of $\omega_o = 0.954 \pm 0.028$ for accumulation particles and $\omega_o = 0.965 \pm 0.023$ for coarse particles;

(d) Sharma et al. (2006), who measured the annual cycle of parameter ω_o at Barrow, finding a maximum of about 0.98 in September, and a wide minimum of 0.94 from February to May;

(e) Ström et al. (2003), who found at Zeppelin (Ny-Ålesund) a set of monthly mean values varying mainly between 0.94 and 0.98 in spring and summer, and between 0.84 and 0.91 in autumn and winter, with a marked minimum in December/January;

(f) Eck et al. (2009), who found at the boreal forest Bonanza Creek site in interior Alaska a set of ω_o (440 nm) values mainly varying between 0.91 and 0.99 in 2004 and 2005, giving an average value equal to ~0.96; and

(g) the ISAC-CNR group, who obtained some accurate estimates of the monthly mean values of ω_o at the Dirigibile Italia station (Ny-Ålesund) during summer 2010, using a pair of Radiance Research M903 nephelometer (to measure the volume scattering coefficient of aerosol particles at the 530 nm wavelength) and Particle Soot Absorption Photometer (PSAP) (to measure the volume absorption coefficient of particles at the

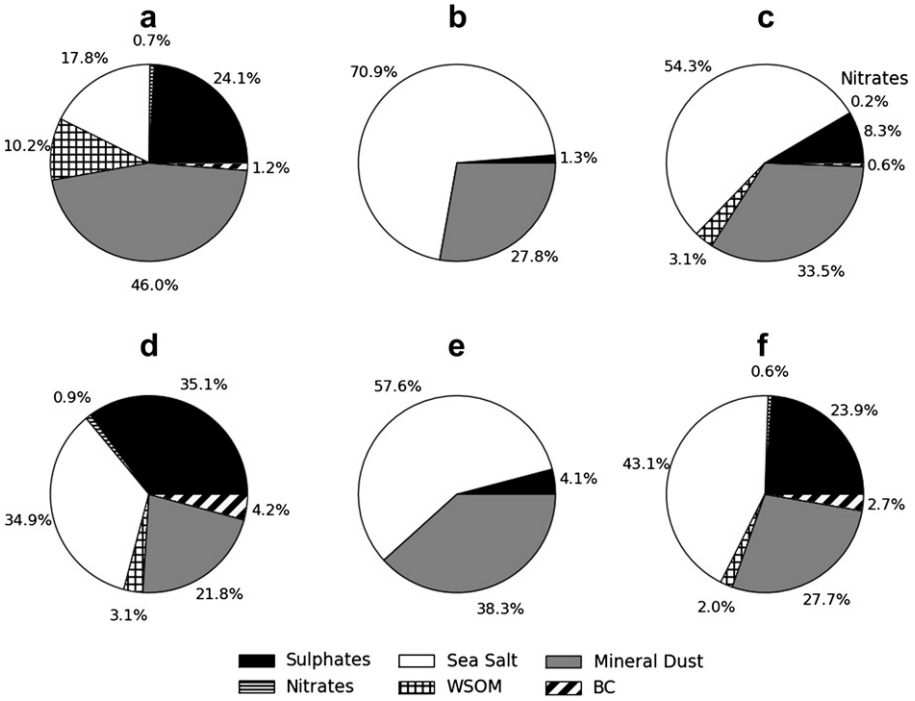

Fig. 10. Upper part: average composition diagrams of the summer ground-level particulate matter sampled at Barrow from June to September for (a) submicron, (b) supermicron, and (c) overall particle size-distributions, pertaining mainly to summer BG aerosol cases. Lower part: as in the upper part for the period from October to May, for (d) submicron, (e) supermicron, and (f) overall particle size-distributions. Different crosshatching patterns are used to indicate the six main particulate matter constituents (WSOM = Water-Soluble Organic Matter; BC = Black Carbon).

467, 530 and 660 nm wavelengths). Over 4500 measurements were performed during the campaign, obtaining a large set of 30-min average values of the volume scattering and absorption coefficients, from which monthly mean values of ω_o (530 nm) were determined, equal to 0.93 ± 0.04 in June, 0.86 ± 0.09 in July, 0.91 ± 0.08 in August, and 0.89 ± 0.09 in September, yielding a seasonal average value of 0.90 ± 0.07.

Such recent measurements of ω_o (530 nm) performed at Ny-Ålesund and the above-mentioned evaluations of ω_o turn out to agree very well with the model-simulated estimates shown in Fig. 11. The exception was the winter–spring data found by Ström et al. (2003) at the Zeppelin station (474 m a.m.s.l.) above Ny-Ålesund, which gave considerably lower values of ω_o probably owing to a higher content of combustion particles measured at the Svalbard site than those sampled at Barrow by Sharma et al. (2002, 2006).

5. Long-term variations of AOD at Antarctic sites over the last decades

Accurate multi-wavelength measurements of AOD have been carried out over the last two decades, employing advanced sun-photometers at the Antarctic stations of Mirny (Russia) (66° 33′ S, 93° 01′ E, 40 m a.m.s.l.), Neumayer (Germany) (70° 38′ S, 8° 15′ W, 40 m a.m.s.l.), Mario Zucchelli (Italy) on the Terra Nova Bay (74° 42′ S, 164° 07′ E, 15 m a.m.s.l.), and South Pole (USA) (89° 59′ S, 139° 16′ E, 2841 m a.m.s.l.). Time series of AOD(500 nm) recorded at Mirny from 1979/1980 to 2005/2006, and Neumayer from 1991 to 2004, and of AOD_{vis} measured at South Pole from 1977 to 2006 with the FWNIP technique were examined by Tomasi et al. (2007), omitting the data measured during the 1982–1984 and the 1991–1994 periods, which were strongly affected by the El Chichón and the Pinatubo (and Cerro Hudson) volcanic eruptions (Herber et al., 1993, 1996). The analysis provided long-term average variations of AOD equal to $-0.09\%\,y^{-1}$ at Mirny, $+0.03\%\,y^{-1}$ at Neumayer, and $-0.01\%\,y^{-1}$ at South Pole, indicating that atmospheric turbidity conditions have been very stable in Antarctica during the past 3 decades, thanks to the great distance of this remote continent from other continental areas, where anthropogenic and biomass burning aerosols are generated.

In the present study, updated series of AOD(500 nm) and AOD_{vis} are presented to provide more recent information on the long-term variations of AOD. They were recorded at:

(1) Mirny, from January 1983 to December 2009, initially using some sun-photometer models equipped with narrow-band interference filters (presenting technical characteristics similar to those described by Sonntag (1970)) and more recently the AARI multispectral sun-photometer having the technical characteristics given in Table 3 (Radionov, 1994, 2005; Radionov et al., 2002);
(2) Neumayer, where multispectral sun-photometer measurements were carried out from January 1991 to April 2004, using the AWI sun-photometer models described in Table 1;
(3) Mario Zucchelli station, where multispectral sun-photometer measurements were performed from December 1987 to January 2005, using different sun-photometer models, whose main technical characteristics are given in Table 3, to collect various seasonal sets of daily values of AOD at various wavelengths, from which the best-fit values of α were calculated (Tomasi et al., 1989, 1991; Vitale and Tomasi, 1990; Di Carmine et al., 2005); and
(4) South Pole, where a time series of AOD_{vis} values was determined by NOAA/GMD from FWNIP measurements routinely performed from January 1977 to December 2010, and an

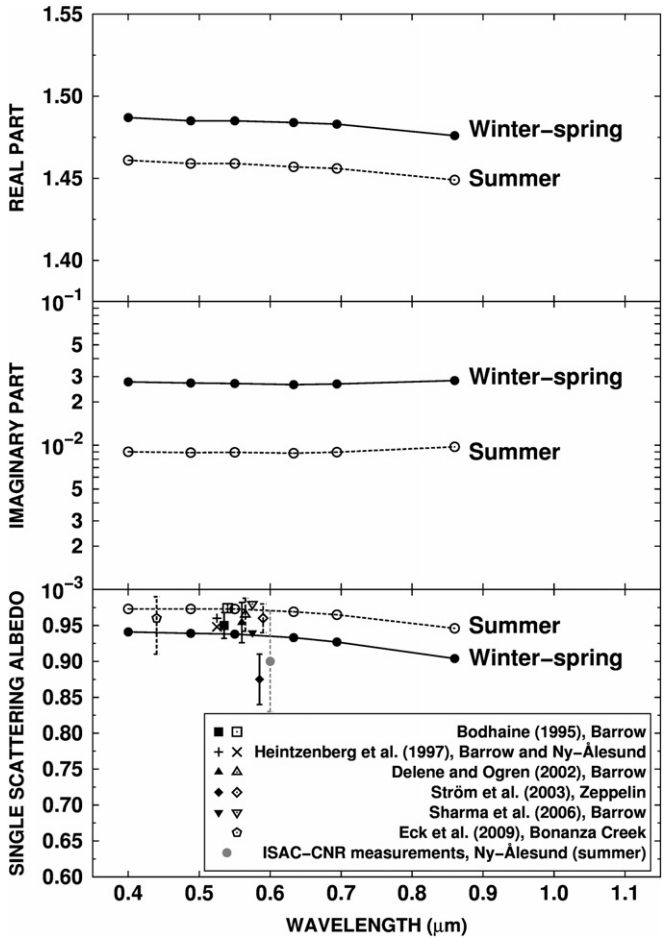

Fig. 11. Spectral curves of (i) real part n_r, (ii) imaginary part n_i of particulate refractive index, and (iii) single scattering albedo ω_o, obtained for the winter–spring and summer models of particulate matter composition at Barrow shown in Fig. 10. The modelled data of ω_o are compared with experimental estimates found in the literature for the Barrow, Ny-Ålesund and mountain Zeppelin stations, and with the recent results derived from field measurements performed by ISAC-CNR at Ny-Ålesund in summer 2010.

additional data-set of AOD and α measurements was recorded by NOAA/GMD from November 2001 to March 2010, using the SP02 sun-photometer model (see Table 1).

Fig. 12 presents the time-patterns of the daily mean values of AOD and α recorded at the 4 Antarctic sites, showing that the daily mean values of AOD(500 nm) measured at coastal sites vary mainly between 0.02 and 0.08, and those measured at South Pole are generally lower than 0.02. Correspondingly, parameter α was found to vary mainly between 0.6 and 1.9 at the coastal sites and between 1.0 and 2.1 at South Pole. The data were analyzed to determine the monthly mean values of AOD(500 nm) and α for the various measurement periods, and were then adjusted for the El Chichón and Pinatubo-Cerro Hudson volcanic eruption effects (Herber et al., 1996). In particular, the monthly mean values of El Chichón's stratospheric contribution to the total atmospheric AOD(500 nm) during the 1982–1986 period were calculated on the basis of the South Pole AOD anomalies evaluated by Dutton and Christy (1992) and Stone (2002), while those due to the Pinatubo and Cerro Hudson extinction effects were estimated according to Stone (2002).

The time series of the monthly mean values of AOD(500 nm) and α obtained at the coastal sites of Mirny, Neumayer and Terra Nova Bay are shown in Fig. 13. The best-fit lines of these time series were drawn obtaining the values of $k = -0.10\%\,y^{-1}$ at Mirny, $k = +0.02\%\,y^{-1}$ at Neumayer, and $k = -0.06\%\,y^{-1}$ at Mario Zucchelli, which differ by no more than $0.03\%\,y^{-1}$ from the slope coefficients estimated by Tomasi et al. (2007), confirming that the BG conditions of Antarctic AOD have continued to remain very stable also over the last decade. The time series of AOD at South Pole are presented in Fig. 14, separately for the FWNIP and SP02 sun-photometer measurements. The regression line drawn for the AOD_{FWNIP} data-set was found to give a nearly null slope coefficient $k = -0.003\%\,y^{-1}$, fully confirming the stability of this parameter over the whole 34-year period from 1977 to 2010. However, it is worth noting that the regression line determined for the SP02 sun-photometer data-set was found to yield a value of $k = +0.17\%\,y^{-1}$ over the period from late 2001 to early 2010, as shown in Fig. 14. This suggests that AOD(500 nm) has slowly increased since 2002, while the time series of α derived from SP02 measurements

Table 3
Main instrumental characteristics of the sun-photometers employed in Antarctica by the AARI group at Mirny (Russia), and the ISAC-CNR group at the "Mario Zucchelli" station, Terra Nova Bay (Italy). The peak wavelengths in bold characters refer to the narrow-band interference filters used to determine the spectral values of AOD, while the peak wavelengths in brackets are those used to measure precipitable water.

Instrumental characteristics	Instruments				
	AARI sun-photometer (Radionov et al., 2002; Radionov, 2005)	ISAC-CNR sun-photometers			
		UVISIR-2 (De Santis et al., 1994	FISBAT (Tomasi et al., 1983)	PREDE POM-01L (Di Carmine et al., 2005)	ASP-15WL (Tomasi et al., 2007)
Spectral range (nm)	395–1041	320–1047	400–1041	400–1020	321–1026
Number of channels	8	12	7	7	15
Peak wavelengths (nm)	**395**, **408**, **479**, **581**, **651**, **789**, **873**, **1041**	320.2, 335.3, 359.8, **401.3**, **459.6**, **505.9**, **550.0**, **671.3**, **780.0**, **865.2**, (939.0), **1047.4**	**400.2**, **441.5**, **500.6**, **550.0**, **669.7**, **868.0** (947.2), **1040.6**	315, **400**, **500**, 675, **870**, 940, **1020**	321.0, 342.0, 370.0, **381.0**, **411.5**, **450.5**, **499.5**, **551.0**, **610.0**, **672.5**, **774.6**, (818.4), **861.2**, (947.7), **1025.7**
Full-width-half-maximum, FWHM (nm)	3.1–10.9	7.2–13.6	8.8–10.7	10	9–12
Entrance optical system	Quartz window	Quartz window	Quartz window	Quartz window	Quartz window
Angular field of view (FOV) diameter	1°	59′–1° 03′	1° 03′–1° 12′	1°	39′–42′
Detector	Silicon photodiode	UDT-555 UV Photop	UDT-500 Photop	Silicon PIN photodiode	UDT-555 UV Photop
Operating temperature	−16 °C to +40 °C	−20 °C to +50 °C	−20 °C to +50 °C	−10 °C to +45 °C	−20 °C to +50 °C
Thermal control	No control	50 °C ± 1 °C	47 °C ± 1 °C	No control	47 °C ± 1 °C
Accuracy of the AOD measurements	0.01	0.01	0.01	0.01	0.01

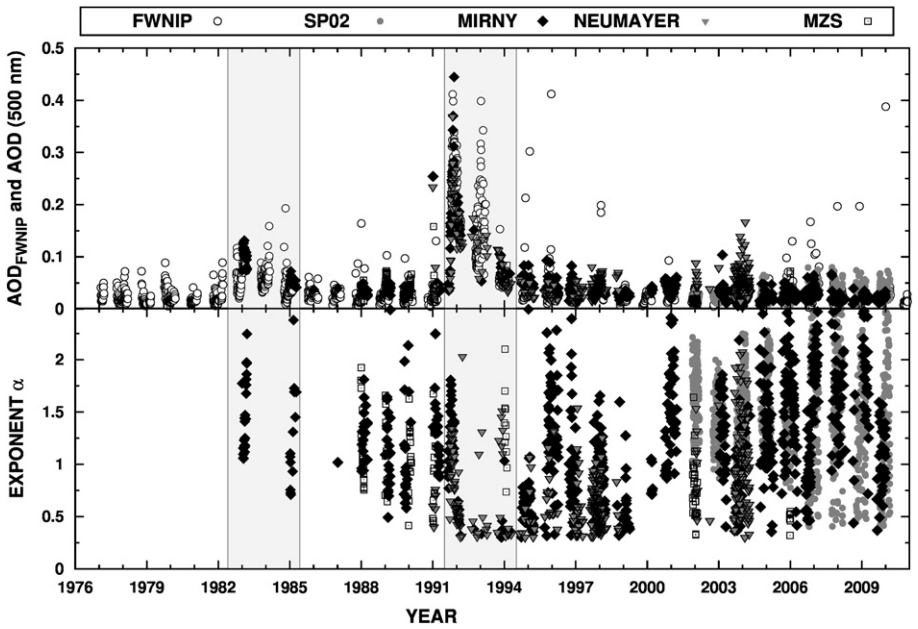

Fig. 12. Upper part: time series of the daily mean values of (i) aerosol optical depth AOD_{FWNIP} (open circles) and AOD(500 nm) (grey circles) obtained at South Pole from the FWNIP and SP02 sun-photometer measurements performed by the NOAA/GMD group, respectively, (ii) AOD(500 nm) sun-photometer measurements taken at Mirny by the AARI group (grey diamonds), (iii) AOD(500 nm) measurements taken at Neumayer by the AWI group (grey downward triangles) using the SPA1 sun-photometer, and (iv) AOD(500 nm) sun-photometer measurements taken at the Mario Zucchelli station, on Terra Nova Bay, by the ISAC-CNR group (open squares) using the sun-photometers described in Table 3. Lower part: time series of the daily mean values of Ångström's exponent α determined from the sun-photometer measurements shown in the upper part. The measurements recorded during the 1982–1984 and 1992–1994 periods for stratospheric particle extinction due to the El Chichón and to the Pinatubo and Cerro Hudson volcanic eruptions, respectively, are evidenced by the grey vertical bands labelled ECAE and PAE.

indicates that a slightly decreasing tendency has occurred, around $-1.8\%\,y^{-1}$, over the last 10 years. The formation of thin layers of stratospheric particles generated by volcanic eruptions at mid-latitudes and subsequently transported towards the austral region could be a plausible explanation for these recent variations in the average time-patterns of AOD and α.

6. Antarctic aerosol radiative properties

Comparing the chemical characteristics and radiative properties of Antarctic aerosols measured at coastal and continental sites in Antarctica, Tomasi et al. (2007) found that large differences exist between the columnar aerosol contents at coastal sites and those

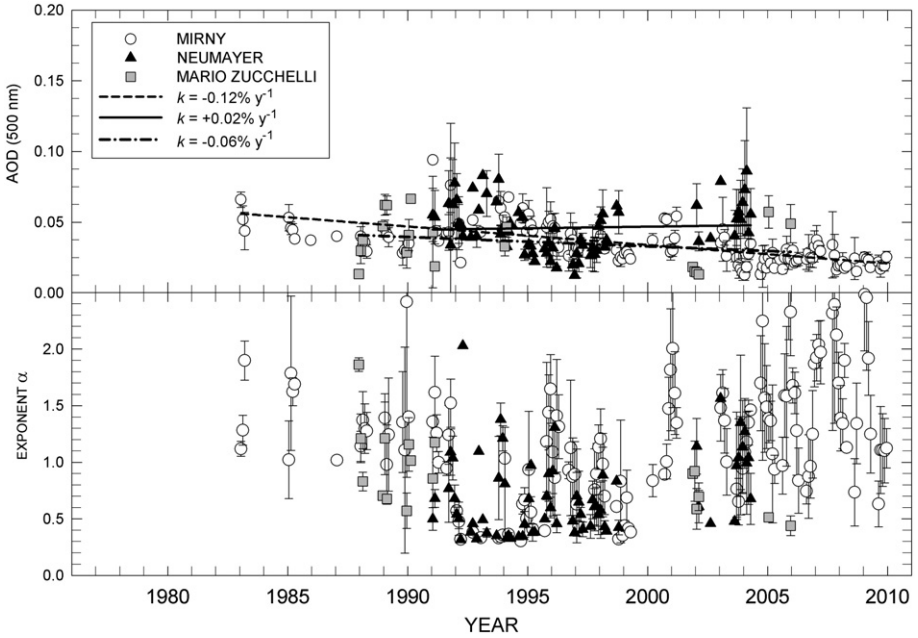

Fig. 13. Upper part: time series of the monthly mean values of AOD(500 nm) obtained with their standard deviations (vertical bars) at (i) Mirny (open circles) by the AARI group (see Table 3), (ii) Neumayer (solid triangles) by the AWI group (see Table 1), and (iii) Mario Zucchelli station (grey squares) on Terra Nova Bay, by the ISAC-CNR group (see Table 3). The regression lines were found to give slope coefficients $k = -0.10\%\,y^{-1}$ at Mirny over the 1983–2009 period (dashed line), $k = +0.02\%\,y^{-1}$ at Neumayer over the 1991–2004 period (solid line), and $k = -0.06\%\,y^{-1}$ at the Mario Zucchelli station over the 1987–2005 period (dashed and dotted line). Lower part: corresponding time series of the monthly mean values of exponent α and their standard deviations, as obtained at the three Antarctic coastal stations.

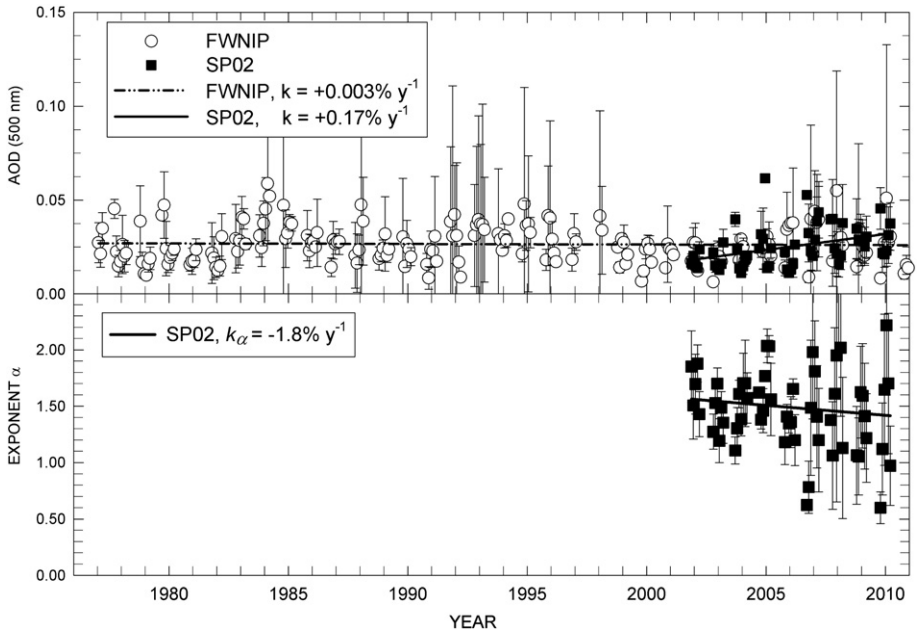

Fig. 14. Upper part: time series of the monthly mean BG values recorded at South Pole of: (i) AOD_{FWNIP} (open circles), given with their standard deviations (vertical bars) obtained from the FWNIP measurements performed by the NOAAGMD group from January 1977 to December 2010, and (ii) AOD(500 nm) (solid squares) obtained from the SP02 sun-photometer measurements performed from November 2001 to March 2010. The regression line drawn for the overall FWNIP data-set was found for a slope coefficient $k = -0.003\%\ y^{-1}$ (dashed and dotted line), while that determined for the SP02 data only has a slope coefficient $k = +0.17\%\ y^{-1}$ (solid line). Lower part: time series of the monthly mean values of exponent α given with their standard deviations, as obtained from the SP02 sun-photometer measurements, giving a best-fit slope coefficient $k_\alpha = -1.8\%\ y^{-1}$ over the observation period from late 2001 to early 2010.

monitored in the inner regions of Antarctic Plateau: (i) the coastal aerosol is strongly influenced by the vicinity of oceanic sources and therefore the particle size-distributions generally contain a strong component of large sea-salt particles during the austral summer, while (ii) the Antarctic Plateau aerosol is most frequently influenced by the subsidence of aerosols from the free troposphere, associated with long-range transport processes (Bigg, 1980), and presents a predominant content of fine nss sulphate and MSA particles (Hara et al., 2004). Thus, significant concentrations of sea-salt aerosols are rarely monitored at South Pole, only in cases when marine air is transported above the station by large storm systems (Shaw, 1988; Bodhaine, 1992).

Taking these differences into account, an attempt was made to define the main chemical composition features of aerosols at the two coastal sites of Mario Zucchelli (Terra Nova Bay, Italy) and Neumayer (Germany), and at the South Pole (USA) high-altitude site, to provide a general picture of the aerosol composition mass fractions and radiative properties in Antarctica:

(1) At Terra Nova Bay, the analysis was performed using the results obtained by Hillamo et al. (1998) from measurements of the mass concentrations of the major inorganic ions present in particulate matter and their atmospheric precursor gases, from late January to mid-February 1995. The percentage mass fractions of the various components (i.e. ions of nss sulphate, nitrate, sea salt, ammonium, Mg, and nss K, Mg and Ca) were determined by Hillamo et al. (1998) separately for the Aitken nuclei, accumulation particle, large particle and coarse particle modes. Combining such data with the more recent evaluations of the mass concentrations of these constituents made by Fattori et al. (2005), the average mass fractions of the particle components were determined, integrating them with evaluations of mineral dust concentration derived from the nss K, Mg and Ca ionic concentrations, and with average BC and OC concentrations assumed to be similar to those evaluated on average by Wolff and Cachier (1998) at Halley Bay during the austral summer.

(2) At Neumayer, the chemical composition of particulate matter was derived from the composition data determined by Weller and Wagenbach (2007), Weller et al. (2008) and Weller and Lampert (2008). These data were then combined with the Wolff and Cachier (1998) estimates of BC and OC concentrations, to define the average percentage mass concentrations of nitrates, sulphates, sea salt, mineral dust, BC and OC, during the austral summer.

(3) At South Pole, several measurements of particulate chemical composition were considered, giving the austral summer concentrations of sulphate, nitrate, ammonium, chlorine, sodium, and nss sulphate ions, MSA, and crustal matter (Tuncel et al., 1989; Arimoto et al., 2004; Piel et al., 2006).

Using the average concentrations derived from the above data-sets and the BC and OC average concentrations proposed by Wolff and Cachier (1998) for this high-altitude site, the percentage mass fractions of particulate matter components were calculated at the three Antarctic sites in terms of nitrate, sulphate, sea salt, mineral dust, BC, OC and VOC-derived concentrations. The average composition diagrams of the particulate matter composition obtained for the austral summer samples examined above are presented in Fig. 16, showing that the predominant fraction is given by sea salt at both coastal sites, with percentages appreciably greater than 50% and lower fractions of sulphates and mineral dust. At South Pole, nss sulphates and MSA-derived compounds constitute about 2/3 of the overall particulate matter, while sea-salt content only just exceeds 10%. Therefore, the present results yield a lower sulphate concentration and an intermediate sea-salt concentration compared to those assumed by Six et al. (2004) at Dome C, consisting of 70% sulphates and 30% sea salt, and those of

Hess et al. (1998) in the Antarctic Plateau model of the OPAC code presenting mass fractions of 91% sulphates, 4.5% sea salt and 4.5% mineral dust.

For the mass fractions of sulphates, nitrates, sea salt, mineral dust, water-soluble organic matter (WSOM) and Black Carbon (BC) shown in Fig. 15, the spectral patterns of parameters n_r, n_i and ω_o were calculated, using the same spectral values of the three optical parameters considered in Fig. 11 for the Arctic data, as proposed by Toon and Pollack (1976) for sulphates, Tang and Munkelwitz (1996) for nitrates, Shettle and Fenn (1979) for sea salt, and Vermote et al. (1997) in the 6S radiative transfer code for the mineral dust, BC and WSOM. The values of real part n_r obtained from the particulate composition models of Fig. 15 are very similar at the two coastal sites – equal to about 1.45 in both cases – due to predominant effects of sea-salt particles. The values of imaginary part n_i at the two coastal sites are also similar, varying between 0.003 and 0.005, and indicating moderate absorption properties leading to values of ω_o ranging between 0.96 and 0.98 at the visible wavelengths. At South Pole, higher values of both n_r and n_i were obtained, substantially due to the higher mean concentration of sulphates and the lower mean concentration of sea-salt particles.

Fig. 16 shows the comparison of the results obtained for the chemical composition models in Fig. 15 with the evaluations of optical parameters n_r, n_i and ω_o found in the literature for various coastal Antarctic sites and South Pole. In particular, the following estimates of n_r and n_i are presented in Fig. 16 for comparison, as obtained by:

(a) Virkkula et al. (2006a,b), who examined sets of optical and chemical measurements performed at the Finnish station of Aboa (73° 03′ S, 13° 25′ W, 400 m a.m.s.l.), and determined values of n_r at visible wavelengths increasing from about 1.46 for fine particles of 0.2–0.6 μm sizes to ~1.56 for coarse particles with sizes >8 μm, from which average values of n_r ranging between 1.44 and 1.46 were obtained at the visible wavelengths, associated with values of n_i close to 0.01; and

(b) Hogan et al. (1979), who found a value of $n_r = 1.54 \pm 0.04$ at South Pole, for particle samples taken in the 0.3–12 μm size range, presenting composition data similar to those shown in Fig. 15 for the South Pole site.

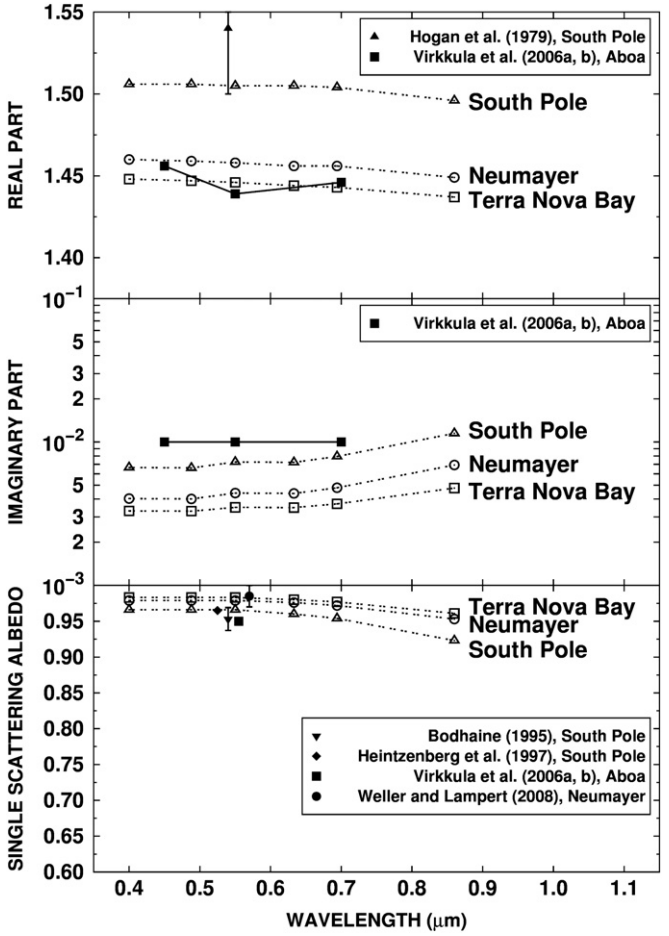

Fig. 16. Spectral curves of (i) real part n_r, (ii) imaginary part n_i of particulate refractive index, and (iii) single scattering albedo ω_o, obtained for the particulate matter composition schemes defined in Fig. 15 from sampling measurements performed in austral summer at Neumayer, Terra Nova Bay and South Pole. The modelled data of n_r and n_i are compared with the experimental evaluations of Hogan et al. (1979) at South Pole and of Virkkula et al. (2006a,b) at Aboa, while the modelled values of ω_o are compared with experimental estimates found in the literature for the Neumayer, Terra Nova Bay and South Pole stations.

The two sets of experimental data turn out to agree substantially with the model-simulated data. The modelled spectral values of ω_o are compared in Fig. 16 with the results obtained by: (a) Virkkula et al. (2006a,b) at Aboa, giving values of ω_o higher than 0.95 for about 93% of the measurements performed at this Antarctic site and lower than 0.90 for only 3.5% of the data; (b) Weller and Lampert (2008) at Neumayer, providing values of ω_o varying in the visible between 0.97 and 1 for more than 95% of the measurements; (c) Bodhaine (1995) at South Pole, with monthly

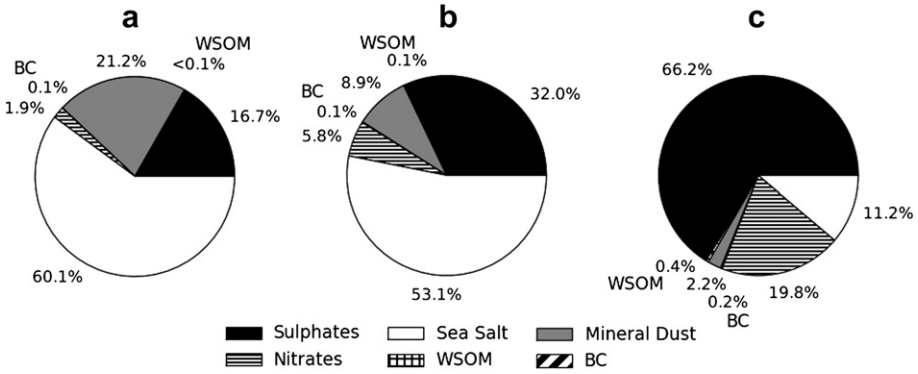

Fig. 15. Average composition diagrams of the overall size-distribution of aerosol particles determined from samples taken during the austral summer at the three Antarctic stations of (a) Mario Zucchelli, on Terra Nova Bay, (b) Neumayer, and (c) South Pole. Different crosshatching patterns are used to indicate the six main particulate matter constituents (WSOM = Water-Soluble Organic Matter; BC = Black Carbon).

median values of ω_o derived from a 3-year set of nephelometer and aethalometer measurements, giving an annual median value of 0.974, and monthly median values varying during the austral summer between 0.942 in January and 0.972 in November, from which a median seasonal value of 0.953 ± 0.016 was obtained; and (d) Heintzenberg et al. (1997) at South Pole, with an annual average value of $\omega_o = 0.965$ in the visible. The comparison in Fig. 16 between modelled and experimental data shows a good agreement for the three optical parameters defined at the coastal sites and South Pole.

7. Conclusions

The present analysis of updated time series of AOD measurements performed at Ny-Ålesund and Barrow shows that an appreciable increase in AOD has been recorded over the past decade, altering the evaluations of the long-term average variation of this optical parameter from values of around $-2.0\%\ y^{-1}$ found by Tomasi et al. (2007) in the 1977–2006 period to nearly null values over the past decade. The measurements of AOD(500 nm) performed with the AWI sun-photometer at Ny-Ålesund and with the SP02 sun-photometer at Barrow over the last 10 years are found to be consistent with the AERONET measurements of AOD(500 nm) performed at Hornsund (Svalbard) and Barrow. Such variation was plausibly due to the increasing emissions of anthropogenic SO_2 from coal-burning and industrial activities in Eurasia since 2000, which have caused the formation of sulphate particle loadings subsequently transported towards the Arctic (Hirdman et al., 2010). In addition, a weak increase in the stratospheric aerosol optical depth has probably occurred over recent years as a result of the exchange of sulphate aerosols and gases between the troposphere and low stratosphere at tropical latitudes, then transported globally and, hence, also towards the polar regions (Hofmann et al., 2009).

More generally, it can be concluded that the recent increase in the SO_2 emissions from Eurasian sources and the subsequent intrusions of anthropogenic aerosol loadings may have caused an increase in the AOD values recorded during the winter–spring months of past years at the Arctic sites. For favourable dynamical conditions, long-lived aerosol of natural and anthropogenic origin can be transported episodically from mid- to high-latitudes during the winter months, and then trapped within the Arctic vortex. These particles accumulate and grow during their life, being subject to variations in chemical composition similar to those measured by Quinn et al. (2007) and Sharma et al. (2002, 2006). The analysis of the monthly mean values of AOD obtained from the data collected during AH episodes indicates that both magnitude of AOD and frequency of AH episodes have been subject to large fluctuations from one season to another, without presenting a stable long-term variation in AOD. However, a slight increase in the seasonal average AOD and a moderate increase in the AH occurrence frequency have been observed during the past decade, presumably as a result of the increasing emissions of pollutant gases in Europe and Asia and the variability of the transport processes from the mid-latitude to the Arctic regions.

No major variations in the average time-patterns of AOD at Antarctic sites were found during the present analysis of updated series of AOD sun-photometer measurements, with respect to the results of Tomasi et al. (2007): the updated values of slope coefficient k, giving a measure of the long-term average variation of AOD(500 nm), were found to vary within $\pm 0.1\%\ y^{-1}$ at the coastal sites and South Pole. Only over the past decade has a slight increase in AOD been observed at South Pole ($k = +0.2\%\ y^{-1}$), associated with a simultaneous appreciable decrease of exponent α from average values of ~ 1.5 to less than 1.3. These features suggest that an increase in the optical density of background stratospheric particle layers could be responsible for such changes in the particulate extinction features of the Antarctic atmosphere, which can better be appreciated at South Pole, where the overall tropospheric AOD generally assumes considerably lower values than at the coastal sites.

The stable values of AOD measured at Antarctic sites provide a useful information for evaluating the radiative forcing effects induced by polar aerosols at both TOA and surface levels. The estimates of the relative concentrations of the main particulate constituents at coastal sites (among which sea-salt particles prevail), and at South Pole (where nss sulphate particles are clearly predominant) are suitable for obtaining more precise evaluations of the direct radiative effects induced by polar aerosols within the surface-atmosphere system: these effects are particularly important for climate studies in Antarctica, bearing in mind that this polar region presents high reflectance conditions in the snow- and ice-covered sea and land areas that efficiently contribute to reflecting solar radiation towards space, thus enhancing the planetary albedo.

Acknowledgements

The research activity was supported by the Programma Nazionale di Ricerche in Antartide (PNRA) and developed as a part of Subproject 2006/6.01: “POLAR-AOD: a network to characterize the means, variability and trends of the climate-forcing properties of aerosols in polar regions”. The authors thank R. Wagener, Principal Investigator of the Barrow AERONET site, for his effort in establishing and maintaining the activities at this important station of the Arctic region. The International Centre for Theoretical Physics, Trieste (Italy) is gratefully acknowledged for its support of the participation of B. Petkov in the framework of the Programme for Training and Research in Italian Laboratories.

References

Ångström, A., 1964. The parameters of atmospheric turbidity. Tellus 16, 64–75.
Arimoto, R., Hogan, A., Grube, P., Davis, D., Webb, J., Schloesslin, C., Sage, S., Raccah, F., 2004. Major ions and radionuclides in aerosol particles from the South Pole during ISCAT-2000. Atmospheric Environment 38, 5473–5484.
Bernhard, G., Booth, C.R., Ehramjian, J.C., Stone, R., Dutton, E.G., 2007. Ultraviolet and visible radiation at Barrow, Alaska: climatology and influencing factors on the basis of version 2. National Science Foundation network data. Journal of Geophysical Research 112, D09101. doi:10.1029/2006JD007865.
Bigg, E.K., 1980. Comparison of aerosol at four baseline atmospheric monitoring stations. Journal of Applied Meteorology 19, 521–533.
Blanchet, J.P., 1995. Mechanisms of direct and indirect climate forcing by aerosol in the Arctic region. In: Charlson, R.J., Heintzenberg, J. (Eds.), Aerosol Forcing of Climate. John Wiley and Sons, New York, pp. 109–121.
Bodhaine, B.A., 1992. The U.S. aerosol monitoring program in Antarctica. SIF Conference Proceedings 35, 15–25.
Bodhaine, B.A., 1995. Aerosol absorption measurements at Barrow, Mauna Loa and the South Pole. Journal of Geophysical Research 100 (D5), 8967–8975.
Bodhaine, B.A., Dutton, E.G., 1993. A long term decrease in arctic haze at Barrow, Alaska. Geophysical Research Letters 20, 947–950.
Charlson, R.J., Schwartz, S.E., Hales, J.M., Cess, R.D., Coakley Jr., J.A., Hansen, J.E., Hofmann, D.J., 1992. Climate forcing by anthropogenic aerosols. Science 255, 423–430.
Chylek, P., Coakley Jr., J.A., 1974. Aerosols and climate. Science 183, 75–77.
Chylek, P., Lohmann, U., Dubey, M., Mishchenko, M., Kahn, R., Ohmura, A., 2007. Limits on climate sensitivity derived from recent satellite and surface observations. Journal of Geophysical Research 112, D24S04. doi:10.1029/2007JD008740.
Damoah, R., Spichtinger, N., Forster, C., James, P., Mattis, I., Wandinger, U., Beirle, S., Wagner, T., Stohl, A., 2004. Around the world in 17 days – hemispheric-scale transport of forest fire smoke from Russia in May 2003. Atmospheric Chemistry and Physics 4, 1311–1321.
Delene, D.J., Ogren, J.A., 2002. Variability of aerosol optical properties at four North American surface monitoring sites. Journal of the Atmospheric Sciences 59, 1135–1150.
De Santis, L.V., Tomasi, C., Vitale, V., 1994. Characterization of Ångström's turbidity parameters in the Po Valley area for summer conditions of the atmosphere. Il Nuovo Cimento 17C, 407–430.
Di Carmine, C., Campanelli, M., Nakajima, T., Tomasi, C., Vitale, V., 2005. Retrievals of Antarctic aerosol characteristics using a Sun-sky radiometer during the

2001–2002 austral summer campaign. Journal of Geophysical Research 110, D13202. doi:10.1029/2004JD005280.
Dutton, E.G., Christy, J.R., 1992. Solar radiative forcing at selected locations and evidence for global lower tropospheric cooling following the eruptions of El Chichon and Pinatubo. Geophysical Research Letters 19, 2313–2316.
Dutton, E., Anderson, G., Carbaugh, G., Jackson, D., Longenecker, D., Nelson, D., O'Neill, M., Stone, R., Treadwell, J., Wendell, J., 2004. Solar and thermal atmospheric radiation CMDL Summary Report 27, pp. 76–96. Global Monitoring Division, Earth System Research Laboratory, NOAA. Boulder, Colorado, pp. 76–96.
Eck, T.F., Holben, B.N., Reid, J.S., Sinyuk, A., Hyer, E.J., O'Neill, N.T., Shaw, G.E., Vande Castle, J.R., Chapin, F.S., Dubovik, O., Smirnov, A., Vermote, E., Schafer, J.S., Giles, D., Slutsker, I., Sorokine, M., Newcomb, W.W., 2009. Optical properties of boreal region biomass burning aerosols in central Alaska and seasonal variation of aerosol optical depth at an Arctic coastal site. Journal of Geophysical Research 114, D11201. doi:10.1029/2008JD010870.
Fattori, I., Becagli, S., Bellandi, S., Castellano, E., Innocenti, M., Mannini, A., Severi, M., Vitale, V., Udisti, R., 2005. Chemical composition and physical features of summer aerosol at Terra Nova Bay and Dome C, Antarctica. Journal of Environmental Monitoring 7, 1265–1274.
Forster, C., Wandinger, U., Wotawa, G., James, P., Mattis, I., Althausen, D., Simmonds, P., O'Doherty, S., Jennings, S.G., Kleefeld, C., Schneider, J., Trickl, T., Kreipl, S., Jäger, H., Stohl, A., 2001. Transport of boreal forest fire emissions from Canada to Europe. Journal of Geophysical Research 106, 22887–22906.
Hara, K., Osada, K., Kido, M., Hayashi, M., Matsunaga, K., Iwasaka, Y., Yamanouchi, T., Hashida, G., Fukatsu, T., 2004. Chemistry of sea-salt particles and inorganic halogen species in Antarctic regions: compositional differences between coastal and inland stations. Journal of Geophysical Research 109, D20208. doi:10.1029/2004JD004713.
Haywood, J.M., Jones, A., Clarisse, L., Bourassa, A., Barnes, J., Telford, P., Bellouin, N., Boucher, O., Agnew, P., Clerbaux, C., Coheur, P., Degenstein, D., Braesicke, P., 2010. Observations of the eruption of the Sarychev volcano and simulations using the HadGEM2 climate model. Journal of Geophysical Research 115, D21212. doi:10.1029/2010JD014447.
Heintzenberg, J., Charlson, R.J., Clarke, A.D., Liousse, C., Ramaswamy, V., Shine, K.P., Wendisch, M., Helas, G., 1997. Measurements and modelling of aerosol single-scattering albedo: progress, problems and prospects. Contributions to Atmospheric Physics 70, 249–263.
Herber, A., Thomason, L.W., Dethloff, K., Viterbo, P., Radionov, V.F., Leiterer, U., 1996. Volcanic perturbation of the atmosphere in both polar regions: 1991–1994. Journal of Geophysical Research 101, 3921–3928.
Herber, A., Thomason, L.W., Radionov, V.F., Leiterer, U., 1993. Comparison of trends in the tropospheric and stratospheric aerosol optical depths in the Antarctic. Journal of Geophysical Research 98, 18,441–18,447.
Herber, A., Thomason, L.W., Gernandt, H., Leiterer, U., Nagel, D., Schulz, K., Kaptur, J., Albrecht, T., Notholt, J., 2002. Continuous day and night aerosol optical depth observations in the Arctic between 1991 and 1999. Journal of Geophysical Research 107 (D10), 4097. doi:10.1029/2001JD000536.
Hess, M., Koepke, P., Schult, I., 1998. Optical properties of aerosols and clouds: the software package OPAC. Bulletin of the American Meteorological Society 79, 831–844.
Hillamo, R., Allegrini, I., Sparapani, R., Kerminen, V.-M., 1998. Mass size distributions and precursors gas concentrations of major inorganic ions in Antarctic aerosol. International Journal of Environmental Analytical Chemistry 71, 353–372.
Hirdman, D., Sodemann, H., Eckhardt, S., Burkhart, J.F., Jefferson, A., Mefford, T., Quinn, P.K., Sharma, S., Ström, J., Stohl, A., 2010. Source identification of short-lived air pollutants in the Arctic using statistical analysis of measurement data and particle dispersion model output. Atmospheric Chemistry and Physics 10, 669–693. www.atmos-chem-phys.net/10/669/2010/.
Hoffmann, A., 2010. Lidar observations of volcanic aerosol layers in the Arctic. Oral Presentation at the IPY Oslo Science Conference, June 11, 2010 (pdf version, private communication).
Hoffmann, A., Ritter, C., Stock, M., Maturilli, M., Eckhardt, S., Herber, A., Neuber, R., 2010. Lidar measurements of the Kasatochi aerosol plume in August and September 2008 in Ny-Ålesund, Spitsbergen. Journal of Geophysical Research 115, D00L12. doi:10.1029/2009JD013039.
Hofmann, D., Barnes, J., O'Neill, M., Trudeau, M., Neely, R., 2009. Increase in background stratospheric aerosol observed with lidar at Mauna Loa Observatory and Boulder, Colorado. Geophysical Research Letters 36, L15808. doi:10.1029/2009GL039008.
Hogan, A.W., Barnard, S., Bortiniak, J., 1979. Physical properties of the aerosol at the South Pole. Geophysical Research Letters 6, 845–848.
Holben, B.N., Eck, T., Slutsker, I., Tanré, D., Buis, J.P., Setzer, A., Vermote, E.F., Reagan, J.A., Kaufman, Y.J., Nakajima, T., Lavenu, F., Jankowiak, I., Smirnov, A., 1998. AERONET – a federated instrument network and data archive for aerosol characterization. Remote Sensing of Environment 66 (1), 1–16.
Holland, M.M., Bitz, C.M., Temblay, B., 2006. Future abrupt reductions in the summer Arctic sea ice. Geophysical Research Letters 33, L23503. doi:10.1029/2006GL028024.
Jaffe, D., Iversen, T., Shaw, G.E., 1995. Comment on "A long term decrease in arctic haze at Barrow, Alaska" by B. A. Bodhaine and E. G. Dutton. Geophysical Research Letters 22, 739–740.
Kravitz, B., Robock, A., Bourassa, A., 2010. Negligible climatic effects from the 2008 Okmok and Kasatochi volcanic eruptions. Journal of Geophysical Research 115, D00L05. doi:10.1029/2009JD013525.
Kravitz, B., Robock, A., Bourassa, A., Deshler, T., Wu, D., Mattis, I., Finger, F., Hoffmann, A., Ritter, C., Bitar, L., Duck, T., Barnes, J., 2011. Simulation and observations of stratospheric aerosols from the 2009 Sarychev volcanic eruption. Journal of Geophysical Research 116, D18211. doi:10.1029/2010JD015501.
O'Neill, N.T., Perro, C., Saha, A., Lesins, G., Duck, T.J., Eloranta, E.W., Nott, G.J., Hoffmann, A., Karumudi, M.L., Ritter, C., Bourassa, A., Abboud, I., Carn, S.A., Savastiouk, V., 2012. Properties of Sarychev sulphate aerosols over the Arctic. Journal of Geophysical Research 117, D04203. doi:10.1029/2011JD016838.
Piel, C., Weller, R., Huke, M., Wagenbach, D., 2006. Atmospheric methane sulfonate and non-sea-salt sulfate records at the European Project for Ice Coring in Antarctica (EPICA) deep-drilling site in Dronning Maud Land, Antarctica. Journal of Geophysical Research 111, D03304. doi:10.1029/2005JD006213.
Polissar, A.V., Hopke, P.K., Paatero, P., Malm, W.C., Sisler, J.F., 1998. Atmospheric aerosol over Alaska. 2. Elemental composition and sources. Journal of Geophysical Research 103 (D15), 19,045–19,057.
Prata, A.J., Carn, S.A., Stohl, A., Kerkmann, J., 2007. Long range transport and fate of a stratospheric volcanic cloud from Soufrière Hills volcano Montserrat. Atmospheric Chemistry and Physics 7, 5093–5103.
Quinn, P.K., Miller, T.L., Bates, T.S., Ogren, J.A., Andrews, E., Shaw, G.E., 2002. A 3-year record of simultaneously measured aerosol chemical and optical properties at Barrow, Alaska. Journal of Geophysical Research 107. doi:10.1029/2001JD001248.
Quinn, P., Shaw, G., Andrews, E., Dutton, E.G., Ruoho-Airola, T., Gong, S.L., 2007. Arctic haze: current trends and knowledge gaps. Tellus 59B, 99–114.
Radionov, V.F., 1994. Variability of aerosol extinction of solar radiation in Antarctica. Antarctic Science 6 (3), 419–424.
Radionov, V.F., 2005. Temporal variability of the aerosol optical characteristics of the atmosphere in the Russian Arctic (Historical review). GAW Report 162, WMO TD 1287. In: WMO/GAW Experts Workshop on a Global Surface Based Network for Long Term Observations of Column Aerosol Optical Properties. World Meteorological Organization, Geneva, Switzerland, pp. 82–85.
Radionov, V.F., Marshunova, M.S., 1992. Long-term variations in the turbidity of the Arctic atmosphere in Russia. Atmosphere – Ocean 30 (4), 531–549.
Radionov, V.F., Lamakin, M.V., Herber, A., 2002. Changes in the aerosol optical depth of the Antarctic atmosphere. Izvestiya – Atmospheric and Oceanic Physics 38, 179–183.
Rahn, K.A., Borys, R.D., Shaw, G.E., 1977. The Asian source of Arctic haze bands. Nature 268, 713–715.
Randles, C.A., Russell, L.M., Ramaswamy, V., 2004. Hygroscopic and optical properties of organic sea salt aerosol and consequences for climate forcing. Geophysical Research Letters 31, L16108. doi:10.1029/2004GL020628.
Ricchiazzi, P., O'Hirok, W., Gautier, C., 2005. The effect of non-lambertian surface reflectance on aerosol radiative forcing. In: Fifteenth ARM Science Team Meeting Proceedings, Daytona Beach, Florida, March 14–18, 2005.
Sakerin, S.M., Kabanov, D.M., Rostov, A.P., Turchinovic, S.A., 2009. Portative solar photometer. Pribory i Tekhnika Eksperimenta (Instruments and Experimental Techniques) 2, 181–182 (in Russian).
Schwartz, S.E., Arnold, F., Blanchet, J.-P., Durkee, P.A., Hofmann, D.J., Hoppel, W.A., King, M.D., Lacis, A.A., Nakajima, T., Ogren, J.A., Toon, O.B., Wendisch, M., 1995. Group report: connections between aerosol properties and forcing of climate. In: Charlson, R.J., Heintzenberg, J. (Eds.), Aerosol Forcing of Climate. John Wiley and Sons, New York, pp. 251–280.
Serreze, M.C., Maslanik, J.A., Scambos, T.A., Fetterer, F., Stroeve, J., Knowles, K., Fowler, C., Drobot, S., Barry, R.G., Haran, T.M., 2003. A record minimum arctic ice extent and area in 2002. Geophysical Research Letters 30 (3), 1110. doi:10.1029/2002GL016406.
Sharma, S., Andrews, E., Barrie, L.A., Ogren, J.A., Lavoué, D., 2006. Variations and sources of equivalent black carbon in the high Arctic revealed by long-term observations at Alert and Barrow: 1989–2003. Journal of Geophysical Research 111, D14208. doi:10.1029/2005JD006581.
Sharma, S., Brook, J.R., Cachier, H., Chow, J., Gaudenzi, A., Lu, G., 2002. Light absorption and thermal measurements of black carbon in different regions of Canada. Journal of Geophysical Research 107 (D24), 4771. doi:10.1029/2002JD002496.
Shaw, G.E., 1982. Atmospheric turbidity in the polar regions. Journal of Applied Meteorology 21, 1080–1088.
Shaw, G.E., 1983. Evidence of a central Eurasian source area of Arctic haze in Alaska. Nature 299, 815–818.
Shaw, G.E., 1988. Antarctic aerosols: a review. Reviews of Geophysics 26, 89–112.
Shaw, G.E., Stamnes, K., Hu, Y.X., 1993. Arctic haze: perturbation to the radiation field. Meteorology and Atmospheric Physics 51, 227–235.
Shettle, E.P., Fenn, R.W., 1979. Models for the Aerosols of the Lower Atmosphere and the Effects of Humidity Variations on their Optical Properties. AFGL-TR-79-0214. In: Environmental Research Paper No. 675. NTIS, ADA 085951, 94 pp.
Six, D., Fily, M., Alvain, S., Henry, P., Benoist, J.-P., 2004. Surface characterization of the Dome Concordia area (Antarctica) as a potential satellite calibration site, using SPOT4/Vegetation instrument. Remote Sensing of Environment 89, 83–94.
Solomon, S., Daniel, J.S., Neely III, R.R., Vernier, J.-P., Dutton, E.G., Thomason, L.W., 2011. The persistently variable "background" stratospheric aerosol layer and global climate change. Science 333, 866–870. doi:10.1126/science.1206027.
Sonntag, D., 1970. Ein Panzeraktinometer mit galvanisch erzeugter Thermosaule. Meteorologische Zeitschrift (Z. Meteorol.) 21, 300–307.

Stohl, A., Hittenberger, M., Wotawa, G., 1998. Validation of the Lagrangian particle dispersion model FLEXPART against large scale tracer experiments. Atmospheric Environment 32, 4245–4264.

Stohl, A., Andrews, E., Burkhart, J.F., Forster, C., Herber, A., Hoch, S.W., Kowal, D., Lunder, C., Mefford, T., Ogren, J.A., Sharma, S., Spichtinger, N., Stebel, K., Stone, R., Ström, J., Tørseth, K., Wehrli, C., Yttri, K.E., 2006. Pan-Arctic enhancements of light absorbing aerosol concentrations due to North American boreal forest fires during summer 2004. Journal of Geophysical Research 111, D22214. doi:10.1029/2006JD007216.

Stone, R.S., 1997. Variations in Western Arctic temperatures in response to cloud radiative and synoptic-scale influences. Journal of Geophysical Research 102, 21,769–21,776.

Stone, R.S., 2002. Monitoring aerosol optical depth at Barrow, Alaska, and South Pole; historical overview, recent results and future goals. SIF Conference Proceedings 80, 123–144.

Stone, R.S., Key, J., Dutton, E., 1993. Properties and decay of stratospheric aerosols in the Arctic following the 1991 eruptions of Mount Pinatubo. Geophysical Research Letters 20, 2359–2362.

Stone, R.S., Dutton, E.G., Harris, J.M., Longenecker, D., 2002. Earlier spring snowmelt in northern Alaska as an indicator of climate change. Journal of Geophysical Research 107, D10. doi:10.1029/2000JD000286.

Stone, R.S., Anderson, G.P., Andrews, E., Dutton, E.G., Shettle, E.P., Berk, A., 2007. Incursions and radiative impact of Asian dust in northern Alaska. Geophysical Research Letters 34, L14815. doi:10.1029/2007GL029878.

Stone, R.S., Anderson, G.P., Shettle, E.P., Andrews, E., Loukachine, K., Dutton, E.G., Schaaf, C., Roman III, M.O., 2008. Radiative impact of boreal smoke in the Arctic: observed and modeled. Journal of Geophysical Research 113, D14S16. doi:10.1029/2007JD009657.

Stone, R.S., Herber, A., Vitale, V., Mazzola, M., Lupi, A., Schnell, R.C., Dutton, E.G., Liu, P.S.K., Li, S.-M., Dethloff, K., Lampert, A., Ritter, C., Stock, M., Neuber, R., Maturilli, M., 2010. A three-dimensional characterization of Arctic aerosols from airborne Sun photometer observations: PAM-ARCMIP, April 2009. Journal of Geophysical Research 115, D13203. doi:10.1029/2009JD013605.

Ström, J., Umegård, J., Tørseth, K., Tunved, P., Hansson, H.-C., Holmén, K., Wismann, V., Herber, A., König-Langlo, G., 2003. One year of particle size distribution and aerosol chemical composition measurements at the Zeppelin station, Svalbard, March 2000–March 2001. Physics and Chemistry of the Earth 28, 1181–1190.

Tang, I.N., Munkelwitz, H.R., 1996. Chemical and size effects of hygroscopic aerosols on light scattering coefficients. Journal of Geophysical Research 101, 19,245–19,250.

Tomasi, C., Prodi, F., Sentimenti, M., Cesari, G., 1983. Multiwavelength sun-photometers for accurate measurements of atmospheric extinction in the visible and near-IR spectral range. Applied Optics 22, 622–630.

Tomasi, C., Vitale, V., Tagliazucca, M., 1989. Atmospheric turbidity measurements at Terra Nova Bay during January and February 1988. SIF Conference Proceedings 20, 67–77.

Tomasi, C., Vitale, V., Zibordi, G., 1991. Multiwavelength sun-photometric measurements of the atmospheric turbidity parameters at Terra Nova Bay during January 1990. SIF Conference Proceedings 34, 125–142.

Tomasi, C., Vitale, V., Lupi, A., Di Carmine, C., Campanelli, M., Herber, A., Treffeisen, R., Stone, R.S., Andrews, E., Sharma, S., Radionov, V., von Hoyningen-Huene, W., Stebel, K., Hansen, G.H., Myhre, C.L., Wehrli, C., Aaltonen, V., Lihavainen, H., Virkkula, A., Hillamo, R., Ström, J., Toledano, C., Cachorro, V.E., Ortiz, P., de Frutos, A.M., Blindheim, S., Frioud, M., Gausa, M., Zielinski, T., Petelski, T., Yamanouchi, T., 2007. Aerosols in polar regions: a historical overview based on optical depth and in situ observations. Journal of Geophysical Research 112, D16205. doi:10.1029/2007JD008432.

Toon, O.B., Pollack, J.B., 1976. The optical constants of several atmospheric aerosol species: ammonium sulfate, aluminum oxide, and sodium chloride. Journal of Geophysical Research 81, 5733–5748.

Treffeisen, R., Tunved, P., Ström, J., Herber, A., Bareiss, J., Helbig, A., Stone, R.S., Hoyningen-Huene, W., Krejci, R., Stohl, A., Neuber, R., 2007. Arctic smoke – aerosol characteristics during a record smoke event in the European Arctic and its radiative impact. Atmospheric Chemistry and Physics 7, 3035–3053. doi:10.5194/acp-7-3035-2007.

Tuncel, G., Aras, N.K., Zoller, W.H., 1989. Temporal variations and sources of elements in the South Pole atmosphere. 1. Nonenriched and moderately enriched elements. Journal of Geophysical Research 94 (D10), 13,025–13,038.

Tunved, P., Hansson, H.-C., Kerminen, V.-M., Ström, J., Dal Maso, M., Lihavainen, H., Viisanen, Y., Aalto, P.P., Komppula, M., Kulmala, M., 2006. High natural aerosol loading over boreal forests. Science 312, 261–263.

VanCuren, R.A., Cahill, T.A., 2002. Asian aerosols in North America: frequency and concentration of fine dust. Journal of Geophysical Research 107 (D24), 4804. doi:10.1029/2002JD002204.

Vermote, E., Tanré, D., Deuzé, J.L., Herman, M., Morcrette, J.J., 1997. Second simulation of the satellite signal in the solar spectrum (6S): an overview. IEEE Transactions on Geoscience and Remote Sensing 35, 675–685.

Vernier, J.P., Pommereau, J.P., Garnier, A., Pelon, J., Larsen, N., Nielsen, J., Christensen, T., Cairo, F., Thomason, L.W., Leblanc, T., McDermid, I.S., 2009. Tropical stratospheric aerosol layer from CALIPSO lidar observations. Journal of Geophysical Research 114, D00H10. doi:10.1029/2009JD011946.

Virkkula, A., Teinilä, K., Hillamo, R., Kerminen, V.-M., Saarikoski, S., Aurela, M., Koponen, I.K., Kulmala, M., 2006b. Chemical size distributions of boundary layer aerosol over the Atlantic Ocean and at an Antarctic site. Journal of Geophysical Research 111, D05306. doi:10.1029/2004JD004958.

Virkkula, A., Koponen, I.K., Teinilä, K., Hillamo, R., Kerminen, V.-M., Kulmala, M., 2006a. Effective real refractive index of dry aerosols in the Antarctic boundary layer. Geophysical Research Letters 33, L06805. doi:10.1029/2005GL024602.

Vitale, V., Tomasi, C., 1990. Atmospheric turbidity measurements at Terra Nova Bay with the multispectral sun-photometer model UVISIR. SIF Conference Proceedings 27, 89–104.

Weller, R., Lampert, A., 2008. Optical properties and sulfate scattering efficiency of boundary layer aerosol at coastal Neumayer Station, Antarctica. Journal of Geophysical Research 113 (D16208), 03304. doi:10.1029/2008JD009962.

Weller, R., Wagenbach, D., 2007. Year-round chemical aerosol records in continental Antarctica obtained by automatic samplings. Tellus 59C, 755–765.

Weller, R., Wöltjen, J., Piel, C., Resenberg, R., Wagenbach, D., König-Langlo, G., Kriews, M., 2008. Seasonal variability of crustal and marine trace elements in the aerosol at Neumayer Station, Antarctica. Tellus 60B, 742–752. doi:10.1111/j.1600-0889.2008.00372.x.

Wolff, E.W., Cachier, H., 1998. Concentrations and seasonal cycle of black carbon in aerosol at a coastal Antarctic station. Journal of Geophysical Research 103, 11033–11041.